Atmos. Chem. Phys. Discuss., https://doi.org/10.5194/acp-2018-977
Manuscript under review for journal Atmos. Chem. Phys.
Discussion started: 4 October 2018

Atmospheric Chemistry and Physics Discussions

Contribution of local and remote anthropogenic aerosols to intensification of a record-breaking torrential rainfall event in Guangdong province

Zhen Liu[1,2], Yi Ming[3], Chun Zhao[4], Ngar Cheung Lau[5,2,1], Jianping Guo[6], Steve Hung Lam Yim[5,2,1]

[1]Institute of Space and Earth Information Science, The Chinese University of Hong Kong, Hong Kong, China
[2]Institute of Environment, Energy and Sustainability, The Chinese University of Hong Kong, Sha Tin, N.T., Hong Kong
[3]Geophysical Fluid Dynamics Laboratory/NOAA, Princeton, New Jersey, USA
[4]School of Earth and Space Sciences, University of Science and Technology of China, Hefei, Anhui, China
[5]Department of Geography and Resource Management, The Chinese University of Hong Kong, Sha Tin, N.T., Hong Kong
[6]State Key Laboratory of Severe Weather, Chinese Academy of Meteorological Sciences, Beijing 100081, China

Correspondence to: Steve Hung Lam Yim (steveyim@cuhk.edu.hk)

Abstract. A torrential rainfall case, which happened in Guangdong Province during December 14–16, 2013, broke the historical rainfall record in the province in terms of duration, affected area, and accumulative precipitation. The influence of anthropogenic aerosols on this extreme rainfall event was examined using a coupled meteorology–chemistry-aerosol model. Enhancement of precipitation in the estuary and near the coast up to 33.7 mm was mainly attributed to aerosol–cloud interactions, whereas aerosol-radiation interactions partially compensated 14% of the precipitation increase. Responses of precipitation to changes in anthropogenic aerosols from local (i.e., Guangdong province) and remote (i.e., outside Guangdong province) sources were also investigated through simulations with reduced aerosol emissions from either local or remote sources. Accumulated aerosol concentration from local sources aggregated mainly near the surface and diluted quickly after the precipitation initiated. By contrast, aerosol concentration from remote emissions extended up to 8 km and lasted much longer before decreasing until peak rainfall began, because aerosols were continuously transported by the strong northerly. Although the patterns of precipitation response to remote and local aerosols resembled each other, remote aerosols contributed more than twice the precipitation increase compared with local aerosols, occupying a predominant role. Ten times of the emission sensitivity test resulted in about ten times of $PM_{2.5}$ concentration compared with the control run. The patterns of precipitation and cloud property changes also resembled that in the control run, but with much greater magnitude. The average precipitation in Guangdong province decreased by 1.0 mm but increased by 1.4 mm in the control run. We noted that the reinforced precipitation increase was concentrated within a more narrowed downstream region, whereas the precipitation decrease was more dispersed across the upstream region. This indicates that the excessive aerosols not only suppress rainfall but also change the spatial distribution of precipitation, increasing the rainfall range, thereby potentially exacerbating flood and drought elsewhere. This study highlights the importance of considering aerosols in meteorology to improve extreme weather forecasting. Furthermore, aerosols from remote emissions may outweigh those from local emissions in the cloud invigoration effect.

Atmos. Chem. Phys. Discuss., https://doi.org/10.5194/acp-2018-977
Manuscript under review for journal Atmos. Chem. Phys.
Discussion started: 4 October 2018

Atmospheric Chemistry and Physics Discussions

1 Introduction

Synoptic weather is a key factor driving air pollution events through photochemical, turbulence, wet deposition, and transport processes (Ding et al., 2009; Guo et al., 2017; Liu et al., 2001; Madronich, 1987). Numerous studies have predicted air quality either numerically or statistically based on weather conditions (Dutot et al., 2007; Otte et al., 2005). Few efforts have been made to identify the influence of aerosols on synoptic weather (Ding et al., 2013; Grell et al., 2011), especially in extreme weather cases (Fan et al., 2015; Zhong et al., 2015). However, the climate effects of aerosols have long been analyzed (Hansen et al., 1997; Myhre et al., 2013; Twomey, 1977).

For decades, China has been affected by severe pollution induced by rapid urbanization and economic development (He et al., 2002). The Pearl River Delta (PRD) region, situated on the south coast of China, is one of the most developed and also the most polluted regions. The aerosol optical depth retrieved from the Moderate Resolution Imaging Spectroradiometer is typically higher than 0.6 in Guangzhou, a megacity in the PRD region (Wu et al., 2005).

In addition to reducing visibility and inducing respiratory diseases (Cohen et al., 2015; Gu and Yim, 2016; Chen et al., 2017), high aerosol concentrations can also affect weather and climate through interactions with radiation and clouds (Bollasina et al., 2011; Lau and Kim, 2006; Wang et al., 2011). Aerosols absorb and scatter solar radiation and serve as cloud condensation nuclei and ice nuclei, which are referred to as aerosol–radiation interactions (ARI) and aerosol–cloud interactions (ACI), respectively (IPCC, 2013). Both ARI and ACI influence deep convection and hence precipitation (Fan et al., 2008, 2013; Koren et al., 2004; Liu et al., 2018; Rosenfeld et al., 2008). Liu et al. (2018) found that ARI suppressed deep convection by reducing the relative humidity in the middle–upper troposphere and weakening the upward motion. Fan et al. (2015) revealed that ARI weakened convergence, enhanced atmospheric stability, and suppressed convection in the basin during the daytime. Excess moist static energy was transported to mountains, thus generating heavy rainfall at night. This suppression effect is dramatically modulated by the intensity of synoptic forcing (Zhong et al., 2017). Compared with the effects of ARI, those of ACI on deep convection and precipitation have received more attention and are more controversial in both observational and modeling studies. Increased aerosols can suppress or enhance precipitation depending on environmental conditions such as humidity, cloud type, cloud phase, and vertical wind shear (Khain, 2009; Lee et al., 2008; Tao et al., 2012). Khain (2009) and Fan et al. (2007) have reported that increases in humidity generate more condensate than lost, resulting in more precipitation from deep convective clouds, especially in a polluted environment. Studies have reported that aerosols inhibit precipitation from shallow clouds (Andreae et al., 2004; Chen et al., 2016; Rosenfeld, 2000), whereas they invigorate deep convection with warm (>15°C) cloud bases (Bell et al., 2008; Koren et al., 2010, 2014). By contrast, the slowing autoconversion rate induced by aerosols forms airborne cloud droplets in clouds with bases near or above 0°C when lacking ice nuclei (Cui et al., 2006; Rosenfeld and Woodley, 2000). Fan et al. (2009, 2012) have suggested that increased aerosols enhanced convection under weak wind shear and suppressed convection under strong wind shear by increasing evaporative cooling for an isolated storm. However, the evaporative cooling induced by aerosols has also been found to enhance precipitation under strong wind shear for cloud systems (Lee et al., 2008; Tao et al., 2007).

Few studies have discussed the relative importance of ARI and ACI on deep convection and precipitation. Fan et al. (2008) suggested that the suppressive effects of ARI can outweigh the invigorative effects of ACI on deep convection and precipitation as the absorption of aerosols enhances. Koren et al. (2008) showed that the net effect of two opposite influences, those of ARI and ACI, on clouds over the Amazon depends on the initial cloud fraction. Large cloud cover fractions were mostly invigorated by ACI, whereas small cloud cover fractions were suppressed by ARI. The precipitation enhancement in the downwind area of a polluted environment could be induced mainly by either ARI or ACI (Fan et al., 2015; Zhong et al., 2015). Both studies have focused on summer extreme rainfall cases because most extreme rainfall events occur in summer over China (Fu et al., 2013).

We selected a torrential rainfall case in winter, which broke the record of Guangdong Province since 1951 in terms of duration, affected area, and cumulative rainfall over the PRD region, to further understand the combined effects and relative importance of ARI and ACI on precipitation. Before this heavy rainfall, the PRD region was affected by strong haze with $PM_{2.5}$ concentrations approaching 174 μg m^{-3}. The significant transboundary nature of air pollution in China has been well recognized (e.g., Gu and Yim, 2016). Effects of local and remote aerosol emissions on monsoons and associated precipitation, particularly the Indian summer monsoon, have been examined in recent years (Bollasina et al., 2014; Cowan and Cai, 2011; Guo et al., 2016b; Jin et al., 2016), which was comprehensively reviewed by Li et al. (2016). The effects of local and remote aerosol emissions on extreme rainfall events remain mostly unexplored. A critical question, therefore, is whether aerosols that affected this extreme rainfall case originated from local or remote aerosol emission sources. The remainder of this study proceeds as follows: Section 2 describes the regional model associated with the experimental design as well as the observation datasets of this study. Main findings on the effects of aerosols on the extreme rainfall event are discussed in section 3. The main conclusions are summarized and discussed in section 4.

2 Model configurations and observational datasets

The principal tool for this work was the Weather Research and Forecasting (WRF) model coupled with Chemistry (WRF-Chem) v3.5.1 (Grell et al., 2005), with some recent improvement by the University of Science and Technology of China (Zhao et al., 2013a, 2014, 2016; Hu et al., 2016). The details of the WRF-Chem configuration are documented in section 2.1, followed by model experiment design in section 2.2. The observational datasets used for validating the simulated precipitation performance, along with hourly in situ $PM_{2.5}$ observations are described in section 2.3.

2.1 WRF-Chem

WRF-Chem is a fully online model coupled with gas-phase chemistry mechanisms and aerosol physiochemical modules. In this model, chemical and meteorological components use the same grid coordinates, time steps, transport schemes, and subgrid physics. The meteorological component (WRF) of this coupled model uses an Eulerian dynamical core with a nonhydrostatic solver (Skamarock et al., 2008). Gas-phase chemical reactions are estimated using the carbon bond chemical mechanism

(Zaveri and Peters, 1999). Aerosol physics and chemistry are treated using the Model for Simulating Aerosol Interactions and Chemistry (MOSAIC) scheme (Zaveri et al., 2008) with aqueous chemistry. The aerosol size distribution is represented by four discrete size bins within the MOSAIC scheme: 0.039–0.156 μm, 0.156–0.625 μm, 0.625–2.5 μm, and 2.5–10 μm (Fast et al., 2006). The approach to aerosol dry deposition is based on Binkowski and Shankar (1995). In-cloud (rainout) and below-cloud (washout) removal of aerosols by resolved clouds and precipitation are simulated following Easter et al. (2004) and Chapman et al. (2009), respectively. The transport and wet removal of aerosols by convective clouds are also considered using the Kain–Fritsch (KF) scheme (Kain and Fritsch, 1990) following Zhao et al. (2009, 2013b). The major physical schemes of meteorological components comprise the KF cumulus scheme; the Yonsei University (YSU) planetary boundary layer (PBL) scheme (Hong et al., 2006); the National Center for Environmental Prediction, Oregon State University, Air Force, and Hydrologic Research Lab's (NOAH) land surface model (Chen and Dudhia, 2001); the Morrison two-moment scheme for cloud microphysics (Morrison et al., 2009); and the rapid radiative transfer for global (RRTMG) for both longwave and shortwave radiation schemes (Iacono et al., 2008). Aerosol interactions with shortwave and longwave radiation are incorporated into the model by linking aerosol optical properties, including optical depth, single-scattering albedo, and asymmetry factor, to RRTMG shortwave and longwave schemes, respectively (Zhao et al., 2010, 2011). The effects of ACI are estimated by considering the activation of aerosols to form cloud droplets based on the maximum supersaturation in the Morrison microphysical scheme (Chapman et al., 2009; Yang et al., 2011).

2.2 Experiment design

WRF-Chem simulations were conducted to investigate the effect of aerosols on the extreme rainfall event of December 14–16, 2013, at. Unless otherwise specified, all time points in this study refer to local standard time (LST), which is equal to UTC+8. Two nested grids (one-way nesting) covered most of China (87.47°–131.67° E, 11.42°–41.22° N) and Guangdong province (109.59°–117.32° E, 20.07°–25.62° N) with a horizontal resolution of 20 km and 4 km, respectively (Figure S1). The cumulus scheme was turned off in the inner domain. Both nested grids used 41 vertical levels extending from the surface to 100 hPa. The meteorological initial and boundary conditions (ICs and BCs) were derived from 6-hourly National Center for Environmental Prediction global final analysis data with a horizontal resolution of 1° × 1°. The 6-hourly chemical ICs and BCs were generated from the Model for Ozone and Related Chemical Tracer version 4 (MOZART-4), which is an offline global chemical transport model suited for tropospheric studies, at a horizontal resolution of 1.9° × 2.5° with 56 vertical levels (Emmons et al., 2010). Anthropogenic emissions were obtained from the Emissions Database for Global Atmospheric Research Hemispheric Transport of Air Pollution v2 inventory (Janssens-Maenhout et al., 2015) for the year 2010 with a resolution of 0.1° × 0.1° (http://edgar.jrc.ec.europa.eu/htap_v2/). Biomass burning emission data were extracted from FINN 1.5 (Wiedinmyer et al., 2010). Dust and sea salt emission schemes were updated following Zhao et al. (2010) and Zhao et al. (2013a), respectively. The results showed marginal differences between simulations with and without dust and sea salt emissions (figure not shown) in our study case; possible reasons for this are discussed in section 4.

Six sets of experiments were performed in total (Table 1). To isolate robust signals from the model's natural variations, five ensemble members with perturbed ICs at 3-h intervals were conducted for each experiment. The simulations started from 08Z to 20Z on December 13 with 3-h intervals, and all ended at 02Z on December 17. The simulation before December 14 was for model spin up, and the following analysis focuses on the results from December 14–16. In the first experiment (CTL), current emissions were used in the simulation with both ARI and ACI effects included (Table 1). Following Fan et al. (2015), we scaled the anthropogenic and fire emissions by a factor of 0.1 and performed the CLEAN simulation. It is used to mimic the situation in which the background of aerosol concentrations serve as cloud condensation nuclei before the economic development in China. The differences between CTL and CLEAN denote the total effects of aerosols on this extreme rainfall case. To examine the role and relative importance of ARI and ACI, the ARIoff run was conducted based on CTL run by excluding the ARI effect. Thus, the differences (CTL minus ARIoff and ARIoff minus CLEAN) represent ARI and ACI effects, respectively (Zhong et al., 2015). To distinguish and isolate the effects induced by local (i.e., domain 2, Guangdong province) emissions and remote (i.e., domain 1, outside Guangdong province) emissions, two other experiments were designed that were identical to the CTL run, except for scaling the emissions and chemical ICs and BCs by a factor of 0.1 in domain 1 (hereafter D1 run, Table 1) and domain 2 (hereafter D2 run). Note that the offline chemical BCs extracted from MOZART were only applicable to domain 1. Along with CTL run, these experiments allowed us to interpret and ascertain aerosol-related changes that would have occurred with either local or remote aerosol emissions by observing differences between CTL minus CLEAN and either D2 minus CLEAN or D1 minus CLEAN. To test the sensitivity of precipitation to aerosol concentrations, one more experiment for extreme polluted case was conducted. We scale the emissions and chemical ICs and BCs by a factor of 10 (10×) in parallel to that in CLEAN run.

2.3 Observational datasets

The model-simulated precipitation performance was evaluated with satellite-based precipitation products and in situ rainfall observations.

Climate Prediction Center morphing technique (CMORPH) data produced by the National Oceanic and Atmospheric Administration covering the period from December 2002 to present were used. In this technique, infrared geostationary satellites observe the motion vectors of precipitation patterns to generate half-hourly precipitation estimates by using passive microwave (PMW) sensors. Time-weighted linear interpolation is exploited to morph the shape and intensity of precipitation features when and where PMW data are unavailable. This provides data for global (60° S–60° N) precipitation analysis with a horizontal resolution of 0.07277° (approximately 8 km at the equator) and temporal resolution of 30 minutes. More details of CMORPH products are documented by Joyce et al. (2004).

The in situ hourly precipitation dataset was developed at the National Meteorological Information Center of the China Meteorological Administration (source: http://data.cma.cn). A total of 115 stations were within domain 2. Their locations are represented as colored circles in Figure 2a.

The hourly $PM_{2.5}$ concentration in situ dataset was obtained from the website of the Ministry of Environmental Protection (source: http://106.37.208.233:20035) (Zhang and Cao, 2015). In total, 58 stations were within domain 2. Their locations are denoted as colored circles in Figure 1c.

3 Results

During December 14–16, 2013, there was a rare continuous rainstorm over all of Guangdong Province. The 3-day accumulated rainfall at most stations exceeded 100 mm (Figure 2a), which may benefit winter and spring water usage, promote air cleaning, and reduce forest fire risk. This was the most extreme precipitation event in the province in terms of duration, affected area, and cumulative rainfall in December since the meteorological record of Guangdong province set in 1951 (Deng et al., 2015). The mid-tropospheric flow pattern, with a ridge to the northeast of the Tibet Plateau and a trough over the west of the Indo-China Peninsula, is favorable for cold air moving southward, whereas moist and warm air from the Bay of Bengal and the South China Sea move northward (see Figure 2a of Deng et al., 2015). The persistent meeting of these two flows results in intense convergence (Figure S1b) at lower levels and thus produces torrential rainfall. Before the study case occurred, Guangdong province was affected by severe pollution on December 13. The hourly-averaged $PM_{2.5}$ concentrations exceeded 100 μg m^{-3} in the delta region, peaking at 173.58 μg m^{-3} (Figure 1c). The Canton Tower, the second tallest tower in the world and the landmark of Guangzhou City (denoted by a star in Figure 1c), was almost invisible under this extreme haze (as seen in the photo in Figure 1b). The area to the north of Guangdong province, including Zhejiang, Jiangsu, and Anhui provinces, was blanketed in grey haze in the natural-color satellite image captured by NASA's Terra (Figure 1a). Note the grey haze area was smog, whereas whiter areas with more defined features were clouds. The column-integrated $PM_{2.5}$ concentrations in these areas reached up to 2000 μg m^{-2} during December 14–16, 2013, in the simulated control run. Strong prevailing northeasterly (Figure 1b) winds south of 30° N along the east coast of China indicated a strong East Asian winter monsoon (Chang et al., 2006). The circulation and pollutant patterns were favorable for aerosol transport to the south of China. Built on the observational and modeling works discussed above, we examined in section 3.2 the total effects and relative importance of ARI and ACI on this extreme rainfall event. We also distinguish and isolate the response to local and remote aerosol emissions in section 3.3. In section 3.4, the sensitivity of precipitation to aerosol emissions is explored.

3.1 Rainfall evaluation compared with observational datasets

The model-simulated precipitation performance was evaluated through comparison with in situ observation and satellite data, as shown in Figure 2. The model output and satellite retrievals were interpolated to in situ observation through bilinear interpolation (Figure 2a–2c). Approximately 100 mm of precipitation accumulated during December 14–16, 2013, covering the entirety of Guangdong Province. However, CMORPH satellite data, which are often used to evaluate model rainfall performance, underestimated the precipitation, particularly near the coast. Previous studies have reported that CMORPH products substantially underestimated heavy rainfall (Jiang et al., 2018; Qin et al., 2014) and cold season rainfall (Xie et al.,

2017). The time series of the average rain rate over Guangdong Province revealed a remarkable extreme rainfall event with a lasting rain rate of 2.5 mm h^{-1} on the second and third day; CMORPH data distinctly underestimated rainfall for these days (Figure 2d). The model reproduced a similar magnitude to the observations with an earlier peak in the early morning near 8:00 a.m. on December 15. The initial time and physics schemes including microphysics, land surface, and PBL are tuned to check whether the peak time will be different. However, the rainfall changes are mostly happened in amplitude rather than peak time, thus we conclude the bias may induced by the meteorology boundary conditions from global model. The Taylor diagram for 3-day accumulated rainfall in Figure 2f suggests that the model simulation yielded a higher pattern correlation of 0.50–0.55 and a lower bias of 5%–20% than the CMORPH retrieval did (0.4 and >20% for pattern correlation and bias, respectively). Signs of bias are represented by inverted (negative) or upright (positive) triangles, indicating that the model overestimated the rainfall amount while the satellite products underestimated it. Overall, the model replicated the spatial distribution, time evolution, and the intensity of this extreme rainfall event. Note that all the analyses in the following sections are based on simulation results from domain 2.

3.2 Effects of ARI versus those of ACI

Aerosols can change cloud properties and precipitation through two processes, radiative and microphysical (Graf, 2004; Kaufman and Koren, 2006), which contribute to the largest uncertainty in human-induced climate changes. We attempted to isolate the effects of ARI and ACI and thus investigate their roles and relative importance in this extreme rainfall event. Figure 3 shows the spatial distribution of the daily accumulated precipitation differences for December 14 and 15 between the different scenarios. Because the results on the third day, December 16, illustrate a similar mechanism to those on December 15, our analysis focused on December 15. The differences between scenarios on December 16 are in the supplementary materials for reference (Figure S2). Distinct effects of aerosols appeared during the second day when the rainfall peaked (Figure 3d), but the aerosol concentration differences occurred on the first day, as shown in Figure 4b; this suggests a time lag effect of aerosols on precipitation. On December 15, the domain-averaged precipitation increased by 1.4 mm. A reduction of up to 19.4 mm appeared in northern Guangdong province, whereas an increase of up to 33.7 mm occurred in southern Guangdong province, particularly in the region near the Pearl River estuary and land along the coast. The region 22°–24° N and 112°–115° E, denoted by red boxes in Figure 3, is our focus for the following analysis, because it exhibits prominent rainfall differences (+7.8 mm) on average and covers some of the most advanced city clusters in China including Hong Kong, Shenzhen, and Guangzhou. The corresponding precipitation differences induced by ARI and ACI were −1.3 mm and +9.3 mm, respectively. Positive indicates an increase, and negative indicates a decrease. It is evident that from the pattern of precipitation changes that the net aerosol effects were dominated by ACI during this event. The time series of average precipitation over the red box shows that the model simulations reproduced a rainfall amount comparable to the observation (Figure S3). Compared with the CTL and ARIoff runs, the CLEAN run yielded an analogous time evolution, with less rainfall during the peak time from 8:00 a.m. on December 15 to 10:00 a.m. on December 16. The next question that arose was how ACI can increase the rainfall amount over the region.

Atmos. Chem. Phys. Discuss., https://doi.org/10.5194/acp-2018-977
Manuscript under review for journal Atmos. Chem. Phys.
Discussion started: 4 October 2018

Atmospheric Chemistry and Physics Discussions

Figure 4a shows the time–height cross section of cloud fraction (shading) and $PM_{2.5}$ concentration (contour) in the CTL run. Deep convection, with a cloud base at approximately 500 m and cloud top extending to approximately 14 km, appeared during December 15–16 when peak rainfall occurred. The $PM_{2.5}$ concentrations in Figure 4a portray a sharp contrast before and after the rainfall peak. After the rainfall peaked at near 07Z in Figure S3, aerosols were washed out dramatically by precipitation. However, before the peak, $PM_{2.5}$ concentrations decreased gradually from 40 μg m^{-3} near the surface to 5 μg m^{-3} near 7 km above ground. These aerosols acted as cloud condensation nuclei to promote cloud droplet formation and invigorate convection (Figure 4b and 4c). There was a prominent cloud fraction band increase near 4 km throughout the period. The increase of cloud fraction extended to the upper troposphere, near 14 km, corresponding to the increase of ice cloud shown in Figure 5d and 5f. By contrast, cloud reduction below 2 km from 06Z on December 14 to 12Z on December 15 may be linked to excessive aerosol concentrations and shallow clouds, which led small droplets to evaporate (Gunn and Phillips, 1957; Zhong et al., 2015). The evaporative cooling resulted in weaker updraft, as shown in Figure 5g and 5i. The similarity of cloud fraction changes between Figure 4b and Figure 4c suggests that ACI dominated the total aerosol effect in this event, which is consistent with the previous discussion.

Figure 5a–5c present the aerosol effects on cloud droplet number concentration (CDNC; shading) and cloud effective radius (contour). With aerosols, CDNC increased dramatically accompanied by reduced cloud effective radius near 2 km from 00Z on December 14 to 00Z on December 15, which reduced the efficiency of collision-coalescence between cloud droplets into raindrops (Rosenfeld, 2000; Twomey, 1977). Smaller cloud droplets are more likely to ascend to higher altitudes, where ice precipitation particles can form. Both the cloud ice number concentration (CINC) and ice cloud effective radius increased above the freezing level (approximately 4 km as calculated from CTL simulation, see dashed lines in Figure 4) from 18Z on December 14 (Figure 5d and 5f). The interim processes released substantial latent heat up to 24 K d^{-1} aloft and strengthened the updrafts (Figure 5g and 5i). These changes, in turn, invigorated greater convection (Storer and van den Heever, 2013; Zhong et al., 2015) and resulted in more precipitation in the estuary. Both observational and numerical studies have found this cloud invigoration effect (Altaratz et al., 2014). The effect refers to the processes that increases in aerosols reduce cloud droplet size and suppress coalescence and warm rain, leading to more freezing of cloud droplets associated with latent heat release and enhancing cold rain (Rosenfeld et al., 2008). The coupling between cloud microphysics and dynamics is at the core of this process (Koren et al., 2015). This feedback loop is driven by latent heat release and regulated by the size distribution of cloud droplets, which is related to the first indirect effect of aerosols (Tao et al., 2012).

To further delineate the mechanism of this microphysics–dynamics feedback, the moisture budget tool was implemented based on the hourly model output. The atmospheric moisture balance is expressed as follows:

$$\frac{\partial Q}{\partial t} = E - P + MFC \quad (1)$$

where Q is the column-integrated water vapor in the atmosphere, t is time, E is evaporation, P is precipitation, and MFC is the vertically integrated moisture flux convergence.

Atmos. Chem. Phys. Discuss., https://doi.org/10.5194/acp-2018-977
Manuscript under review for journal Atmos. Chem. Phys.
Discussion started: 4 October 2018

Evaporation is small in areas of intense precipitation and saturation (Banacos and Schultz, 2005). The column-integrated water vapor changes are small (figure not shown), thus precipitation is balanced by the moisture flux convergence as follows:

$$P \approx MFC \quad (2)$$

The spatial distributions of column-integrated MFC (shading) and moisture flux (vector) between CTL and CLEAN on December 15 are displayed in Figure 6a. The MFC pattern was in good agreement with precipitation differences in Figure 3d, suggesting the validity of the derivation of Equation (2). The average MFC change over the analysis region was +8.1 mm, which is comparable to +7.8 mm in precipitation difference. The vertically integrated moisture flux changes followed the wind pattern, as shown in Figure 13d. The moisture was transported by northerly wind over the northeast of Guangdong province and southerly wind over the sea. These flows converged in the estuary and near the coast with a magnitude of approximately 25 kg m^{-1} s^{-1}. The pattern of differences between CTL and CLEAN resembles that between ARIoff and CLEAN (Figure 6), which suggest the dominant effect of ACI. The magnitude of changes over the analysis region was smaller in the former case, indicating the compensation effect between ARI and ACI in this case, as noted in section 3.1.

These findings reveal the prominent effects of aerosols on rainfall amount over the estuary and near the coast in this extreme rainfall event. The pattern of precipitation and associated cloud-related variables in CTL minus CLEAN (total effects) bore a resemblance to that in ARIoff minus CLEAN (ACI effects), which allowed us to ascertain that ACI dominated the total effects. By applying the moisture budget tool, we confirmed the microphysical–dynamic feedback of ACI effects on invigorating convection. Cloud invigoration is the consequence of the following chain of processes. (1) Larger concentrations of cloud droplets with smaller radii are induced by increased aerosols. (2) Collision–coalescence processes slow, and water clouds ascend to freeze into ice clouds. (3) Additional latent heat release enhances horizontal convergence and strengthens upward motion. (4) More vigorous latent heat is released aloft in response to stronger convection. These feedback processes enhance cold rain and result in greater precipitation.

3.3 Local versus remote aerosol emission effects

A crucial question is the extent to which increased anthropogenic aerosols from either local (i.e., domain 2, which denotes Guangdong province) or remote (i.e., domain 1, which denotes outside Guangdong province) sources result in precipitation changes. Previous studies have reported different roles of local and remote aerosol sources in affecting tropical precipitation (Chou et al., 2005) and monsoons associated with precipitation (Bollasina et al., 2014; Cowan and Cai, 2011) from a climate perspective. However, the differing effects of local and remote aerosols on weather, such as extreme rainfall, are rarely explored. In this section, we examine the roles and relative importance of local and remote aerosols in the precipitation increase in the estuary during this extreme rainfall event.

The differences in time–height cross section of cloud fraction (shading) and $PM_{2.5}$ concentration (contour) induced by the effects of local and remote emissions are shown in Figures 7a and 7b, respectively. With local emissions, the aerosol concentrations mainly increased within the PBL below 2 km before 12Z on December 15 (Figure 7b). The accumulated aerosols were washed out quickly after the rainfall initiated. By contrast, with remote emissions, a higher aerosol concentration

extended to approximately 8 km after 3Z on December 14 (Figure 7a). Two peaks near 0.5 km and 5 km above ground were centered near 10Z and 18Z on December 14, respectively, indicating a strong transportation of aerosols. The earlier peak, near 5 km, was caused by strong wind speed in the free atmosphere compared with that within the PBL. Moreover, the aerosol concentrations lasted longer before decreasing dramatically until the peak rainfall started at 07Z on December 15, because aerosols were transported continuously from the remote area. The cloud fraction reduction was coherent with aerosol concentration peaks, indicating that increased aerosols led small cloud droplets to evaporate. Comparing patterns of cloud fraction changes between Figure 7a and 7b and Figure 4b indicates the dominant effects of aerosols from remote areas. The CDNC (shading) increased in both D1 and D2 runs compared with the CLEAN run before the rainfall peak (Figure 8a and 8b). However, the discernible cloud effective radius (contours) decrease appeared only in the D1 run and was attributed to a stronger CDNC increase. Correspondingly, the CINC and ice cloud effective radius showed more remarkable increases in the D1 run during the rainfall peak time (Figure 8c and 8d). The associated latent heat and vertical velocity were much stronger in the D1 run compared with the D2 run (Figure 8e and 8f). As a result, the average precipitation increase over the analysis region on December 15 was 7.3 mm with remote aerosol emissions, much greater than that with local aerosol emissions (3.1 mm, Figure 9c and 9d). These findings suggest that both the effects of local and, to a much greater extent, remote aerosol emissions contribute to precipitation increases over the analysis region.

3.4 Tenfold anthropogenic emissions and chemical ICs and BCs

An optimal aerosol loading should exist in which the convection is the most vigorous (Rosenfeld et al., 2008). For aerosol concentrations below the optimum, the convection is invigorated by smaller droplets; thus, stronger updraft releases larger latent release (Dagan et al., 2015b). By contrast, suppression effects dominate above the optimum (Small et al., 2009). The optimum value is determined by environmental conditions (e.g., relative humidity, see Dagan et al., 2015a). In this section, a tenfold aerosol emission simulation (10×) was conducted to examine the sensitivity of precipitation and associated cloud properties to aerosol concentrations.

The $PM_{2.5}$ concentrations (contours) in 10× increased significantly to approximately ten times that in CTL, indicating a linear relationship from emissions to aerosol concentration (Figure 10). The associated boundary layer cloud formation (shading) was further suppressed below 2 km, which is consistent with the result in Figure 4b. The change patterns in cloud fraction and aerosol concentration in Figure 10 are similar to that in Figure 4b, but Figure 10 shows a much greater magnitude. The CDNC (shading) increase and cloud effective radius (contours) reduction in Figure 11a are also more pronounced than those in Figure 5a. CDNC noticeably decreased below 1.5 km but increased substantially from 1.5 km to 4 km before 4:00 a.m. on December 14. This finding suggests the ascent of cloud droplets, which is attributed to the smaller effective radius induced by excessive aerosols in 10× compared with that in CTL. The smaller cloud droplets favored the formation of deeper convection manifested by more CINC and larger ice cloud effective radii (Figure 11b). The involved latent heat and vertical velocity during the rainfall peak time from 8Z on December 15 to 10Z on December 16 in Figure 11c exhibit a stronger increase associated with a higher altitude above the freezing level than that in Figure 5c. This means that water ascended higher and froze before

precipitating, which led to additional latent heat release. A more salient negative anomaly of latent heat and vertical velocity arose below 4 km from 06Z to 22Z on December 15 and below 10 km from 06Z to 18Z on December 16. This should relate to stronger cloud evaporation and ice melting, as discussed by Rosenfeld et al. (2008). The greater cooling below and greater heating above suggest the intensified upward energy transport. This configuration should enhance updraft above and downdraft below induced by additional warming and cooling respectively, which could further invigorate convection and produce more precipitation (Rosenfeld, 2006). Precipitation on December 15 was suppressed over the upstream region up to 39.6 mm in the northwest of Guangdong province but substantially enhanced up to 59.7 mm over the downstream region near the coastal region (Figure 12b). A similar finding was reported by Zhong et al. (2015). The delay of early rain in the upstream area resulted in more rainfall and stronger rain intensity within the downstream area and a more narrowed region compared with the red box in Figure 3b. The average precipitation in Guangdong province on December 15 decreased by 1.0 mm in 10×, whereas it increased by 1.4 mm in CTL. Tenfold aerosol emissions produced a more polluted environment, with $PM_{2.5}$ concentrations of approximately 300 μg m^{-3}. Although abundant moisture was transported from the Bay of Bengal and the South China Sea (Figure S1b), the aerosol loading may still have surpassed the optimal value for cloud invigoration and thus suppressed precipitation over Guangdong province. Moreover, aside from suppressing the rainfall amount, excessive aerosols also have the potential to redistribute precipitation and increase its range in spatial distribution. With tenfold aerosol emissions, the experiment showed a similar pattern to the CTL run, but the signal was much stronger, implying that the mechanism was consistent with what we discussed before.

4 Summary and discussion

In this study, we found that aerosols significantly affect local extreme weather (i.e., torrential rainfall) by suppressing warm rain and invigorating deep convection induced by the effects of remote emissions through ACI. With aerosols, CDNC increases remarkably, reducing the size of cloud droplets. Smaller cloud droplets are unfavorable to collision–coalescence, which is an essential process for initiating warm rain (Tao et al., 2012). Thus, more cloud water ascends to a higher altitude below the 0°C isotherm to freeze; this is associated with more latent heat release, and convection is invigorated (Rosenfeld et al., 2008). Moreover, additional latent heat release induced by freezing further enhances the upward motion. This feedback between microphysical and dynamic processes results in more rainfall (Tao et al., 2007) up to 33.7 mm in our simulation. On average, ACI enhanced precipitation over the analysis region. Conversely, ARI partially compensated for the precipitation increase by 14%. The analysis of the moisture budget suggests that the precipitation increase was manifested by strengthening the column-integrated MFC. Our finding confirms that microphysical–dynamic feedback is at the core of the effects of ACI on convection invigoration.

An interesting question is why the precipitation increases induced by ACI appear on land near the Pearl River estuary and the coast. Khain et al. (2008) found that aerosols generally suppress cloud formation in relatively dry conditions, whereas they invigorate convection in moist environments. Fan et al. (2009) suggested that wind shear may take a dominant role in regulating

the effects of aerosol on deep convection. Increased aerosols suppress (invigorate) convection under strong (weak) wind shear. These findings highlight the crucial roles of humidity and wind shear in modulating the cloud invigoration effects induced by aerosols. Strong wind shear enhances the entrainment of dry air into clouds and transports cloud liquid to unsaturated regions; this leads to greater evaporation and sublimation of cloud particles. These processes are associated with cooling, downdrafts, and convergence, especially at high aerosol concentrations (Khain, 2009; Lee et al., 2008). The convergence thus fosters secondary cloud formation and contributes to an increase in precipitation. However, Fan et al. (2009) stressed that the net latent heat release, as an energy source for convection, is greater under weak wind shear than under strong wind shear. Aerosols enhance convection under weak wind shear until an optimal aerosol concentration is reached at which the net latent heat release equilibrates. This mechanism may only be applicable to isolated storms rather than to cloud systems. Note that the previous studies have used different wind components (zonal component, meridional component, or total wind) at different heights with different thresholds (e.g., upper limits vary from 10 m s^{-1} to 20 m s^{-1}). These different standards may only suitable for specific environmental conditions, because previous studies have been based on limited cases. In our work, the wind shear was estimated as the difference between the maximum and minimum total wind speeds at 0–10 km. The spatial distribution of wind shear (first row) and column-integrated water vapor (second row) are presented in Figure 13. The wind shear increased with the southeast–northwest tilt ranging from 35 m s^{-1} to 80 m s^{-1} (Figure 13a and 13b). Our definition of wind shear was different from other studies (e.g., Lee et al. 2008; Fan et al. 2009; Li et al. 2011; Guo et al., 2016a), with a higher altitude. We chose 10 km because the latent heat release, which is a key factor determining convection intensity and partly depends on wind shear, extends up to approximately 10 km (Figure 5g). Although the wind shear in our work was stronger than that in other studies with magnitudes lower than 10 m s^{-1}, the aerosol invigoration effect appeared over the region with relatively weak wind shear and high humidity on the land along the coast, as presented in Figure 13. This invigoration effect under weak wind shear for cloud systems was described in a recent work (Li et al., 2011), whereas it was to some extent contradicted by the results of Lee et al. (2008). Conversely, precipitation was suppressed to the northwest of Guangdong, with relatively strong wind shear and low humidity, as shown in Figure 13b and 13d. The gradient of wind shear and humidity increased between the southeast and northwest of domain 2 on December 15 when peak rainfall occurred. The results confirm that the effect of aerosols on precipitation is related to relative humidity and wind shear. However, this relationship remains dependent on the situation and may be affected by other meteorological variables, such as convective available potential energy (Khain et al., 2005), cloud phase (Lin et al., 2006), and cloud type (Koren et al., 2008). The relative importance of different meteorological variables in regulating the aerosol-induced precipitation effect requires both long-term observation and model sensitivity tests to provide a more comprehensive picture.

Aerosol emissions were separated into those from Guangdong Province and those from elsewhere, named experiments D2 and D1, respectively, to represent the effects of local and remote emissions on this extreme rainfall event. The surface aerosol concentrations accumulated slowly from local emissions if the rainfall system came with strong northerlies. Instead, aerosols, transported from remote areas persistently, extended to higher altitudes, up to 8 km. The aerosol concentrations thus were maintained at a relatively high level in the D1 and invigorated convection. The precipitation averaged over the analysis region

on December 15 increased by 7.3 mm from the effects of remote aerosol emissions but only 3.1 mm from local aerosol emissions. These results suggest that the effects of remote aerosol emissions played a dominant role in the intensification of precipitation in the estuary, which implies the potential influence of remote aerosol emissions on extreme synoptic weather events. However, this crucial issue remains insufficiently explored.

Previous studies have suggested an optimal aerosol loading in which condensational heating and evaporative cooling are balanced, leading to the most vigorous convection (Fan et al., 2007, 2009; Rosenfeld et al., 2008; Wang, 2005). A tenfold emission experiment showed a similar pattern with CTL but with a much stronger signal. The greater cooling below and heating above led to enhanced upward heat transport, which could further invigorate convection and result in more precipitation later (Rosenfeld et al., 2008). Excessive aerosols led to more precipitation increases, up to 59.7 mm, which is much larger than the 33.7 mm from CTL. However, the precipitation increase was limited to a more narrowed region along the coast in the downwind area; this may be related to the adequate supply of water vapor from onshore wind, as shown in Figure 13d. The average precipitation over Guangdong province decreased by 1.0 mm in 10× but increased by 1.4 mm in CTL. These results indicate that aerosol concentrations in 10× exceeded the optimal aerosol loading for convection invigoration and instead suppressed the rainfall amount. The retribution for spatial distribution of precipitation with a sharper contrast implies that air pollution may increase the possibility of both flood and drought.

We note that uncertainties exist in aerosol emission and the representation of ACI. Although ice nucleation may have little effect on the spatial distribution and temporal evolution of surface precipitation (Deng et al., 2018), this factor is not yet considered in the WRF-Chem model. This may explain negligible differences in results between simulations with and without dust and sea salt emissions. Additionally, dust sources are far from our analysis region and the prevailing wind is northerly; these produce low dust and sea salt concentrations, respectively. It is noteworthy that we assume the ARI and ACI effects are linear additive as previous studies (Fan et al., 2015; Zhong et al., 2015), so that the ACI effect is derived by subtracting ARI from total aerosol effects. We cannot check the nonlinearity between ARI and ACI effects because it is not easy to turn off ACI effect. The problem is how to set the background concentration of cloud droplet number while keep the ARI as same in control run. This means that we could only prescribe the cloud droplet number concentration rather than adjust the emission or aerosol concentration. However, the ACI effect is very sensitive to the number we set (Gustafson et al., 2007).

Although our findings are limited to a case study, this case is, nevertheless, representative of the remarkable aerosol effect on an extreme rainfall events through ACI. This finding provides more evidence of the importance of considering aerosols in extreme weather (i.e., torrential rainfall) forecasting. More interestingly, aerosols from remote emission sources exhibited the potential to modify extreme weather through transboundary air pollution. This case clearly demonstrates the complicated feedback between the dynamic and microphysical processes induced by aerosols. Aerosols substantially redistributed the rainfall amount, a finding with crucial implications for the availability and usability of water resources in different regions of the world (Li et al., 2011). High aerosol concentrations may intensify both flood and drought by invigorating convection.

Acknowledgment. This work was jointly supported by the Early Career Scheme of Research Grants Council of Hong Kong (grant CUHK24301415), the National Key Basic Research Program of China (grant 2015CB954103), the Ministry of Science and Technology of China (grant 2017YFC1501401), the Improvement on Competitiveness in Hiring New Faculties Fund (2013/2014) of The Chinese University of Hong Kong (CUHK, grant 4930059), and the Vice-Chancellor's Discretionary Fund of the Chinese University of Hong Kong (grant 4930744). The appointment of NCL at the CUHK is supported by the AXA Research Fund. Model simulations were conducted on computer clusters at Geophysical Fluid Dynamics Laboratory (GFDL). Larry Horowitz and Maofeng Liu provided helpful comments. We acknowledge the Global Scholarship Program for Research Excellence 2017–18 at the CUHK for supporting Zhen Liu's exchange visit to Princeton University. Chun Zhao is supported by the Thousand Talents Plan for Young Professionals, the Fundamental Research Funds for the Central Universities, and the National Natural Science Foundation of China (grant 41775146).

References

Altaratz, O., Koren, I., Remer, L. A. and Hirsch, E.: Review: Cloud invigoration by aerosols-Coupling between microphysics and dynamics, Atmos. Res., 140–141, 38–60, doi:10.1016/j.atmosres.2014.01.009, 2014.

Andreae, M. O., Rosenfeld, D., Artaxo, P., Costa, A. A., Frank, G. P., Longo, K. M. and Silva-Dias, M. A. F.: Smoking rain clouds over the Amazon, Science, 303(5662), 1337–1342, doi:10.1126/science.1092779, 2004.

Banacos, P. C. and Schultz, D. M.: The use of moisture flux convergence in forecasting convective initiation: historical and operational perspectives, Weather Forecast., 20(3), 351–366, doi:10.1175/WAF858.1, 2005.

Bell, T. L., Rosenfeld, D., Kim, K. M., Yoo, J. M., Lee, M. I. and Hahnenberger, M.: Midweek increase in U.S. summer rain and storm heights suggests air pollution invigorates rainstorms, J. Geophys. Res. Atmos., 113(2), doi:10.1029/2007JD008623, 2008.

Binkowski, F. S. and Shankar, U.: The regional particulate matter model: 1. Model description and preliminary results, J. Geophys. Res., 100(D12), 26191, doi:10.1029/95JD02093, 1995.

Bollasina, M. A., Ming, Y. and Ramaswamy, V.: Anthropogenic aerosols and the weakening of the South Asian summer monsoon, Science, 334(6055), 502–505, doi:10.1126/science.1204994, 2011.

Bollasina, M. A., Ming, Y., Ramaswamy, V., Schwarzkopf, M. D. and Naik, V.: Contribution of local and remote anthropogenic aerosols to the twentieth century weakening of the South Asian Monsoon, Geophys. Res. Lett., 41(2), 680–687, doi:10.1002/2013GL058183, 2014.

Chang, C.-P., Z. Wang, and H. Hendon: The Asian winter monsoon, The Asian Monsoon, B. Wang, Ed., Springer, 89–127, 2006.

Chapman, E. G., Gustafson, W. I., Easter, R. C., Barnard, J. C., Ghan, S. J., Pekour, M. S. and Fast, J. D.: Coupling aerosol-cloud-radiative processes in the WRF-Chem model: Investigating the radiative impact of elevated point sources, Atmos. Chem. Phys., 9(3), 945–964, doi:10.5194/acp-9-945-2009, 2009.

Chen, F. and Dudhia, J.: Coupling an advanced land surface–hydrology model with the Penn State–NCAR MM5 modeling system. Part I: Model implementation and sensitivity, Mon. Weather Rev., 129(4), 569–585, doi:10.1175/1520-0493(2001)129<0569:CAALSH>2.0.CO;2, 2001.

Chen, T., Guo, J., Li, Z., Zhao, C., Liu, H., Cribb, M., Wang, F. and He, J.: A CloudSat perspective on the cloud climatology and its association with aerosol perturbations in the vertical over Eastern China, J. Atmos. Sci., 73(9), 3599–3616, doi:10.1175/JAS-D-15-0309.1, 2016.

Chen X. C., Jahn H. J., Engling G., Ward T. J., Kraemer A., Ho K. F., Yim S. H. L., Chan C. Y.: Chemical characterization and sources of personal exposure to fine particulate matter ($PM_{2.5}$) in the megacity of Guangzhou, China., Environ. Pollut., 231, 871–881, 2017.

Chou, C., Neelin, J. D., Lohmann, U. and Feichter, J.: Local and remote impacts of aerosol climate forcing on tropical precipitation, J. Clim., 18(22), 4621–4636, doi:10.1175/JCLI3554.1, 2005.

Cohen A J, Brauer M, Burnett R, et al.: Estimates and 25-year trends of the global burden of disease attributable to ambient air pollution: an analysis of data from the Global Burden of Diseases Study, The Lancet, 2017, 389 (10082), 1907-1918, 2015.

Cowan, T. and Cai, W.: The impact of Asian and non-Asian anthropogenic aerosols on 20th century Asian summer monsoon, Geophys. Res. Lett., 38(11), doi:10.1029/2011GL047268, 2011.

Cui, Z. Q., Carslaw, K. S., Yin, Y. and Davies, S.: A numerical study of aerosol effects on the dynamics and microphysics of a deep convective cloud in a continental environment, J. Geophys. Res., 111(D5), D05201, doi:10.1029/2005JD005981, 2006.

Dagan, G., Koren, I. and Altaratz, O.: Aerosol effects on the timing of warm rain processes, Geophys. Res. Lett., 42(11), 4590–4598, doi:10.1002/2015GL063839, 2015a.

Dagan, G., Koren, I. and Altaratz, O.: Competition between core and periphery-based processes in warm convective clouds – from invigoration to suppression, Atmos. Chem. Phys., 15(5), 2749–2760, doi:10.5194/acp-15-2749-2015, 2015b.

Deng, W. J., Wu, N. G., Lin, L. X., and Zhang, H., L.: Causal analysis of an unusual continuous torrential rainfall event in Guangdong in the winter of 2013, Meteor. Sci. Technol., 43(2), 276-282, doi:10.19517/j.1671-6345.2015.02.019, 2015.

Deng, X., Xue, H. and Meng, Z.: The effect of ice nuclei on a deep convective cloud in South China, Atmos. Res., 206, 1–12, doi:10.1016/j.atmosres.2018.02.013, 2018.

Ding, A., Wang, T., Xue, L., Gao, J., Stohl, A., Lei, H., Jin, D., Ren, Y., Wang, X., Wei, X., Qi, Y., Liu, J. and Zhang, X.: Transport of north China air pollution by midlatitude cyclones: Case study of aircraft measurements in summer 2007, J. Geophys. Res. Atmos., 114(8), doi:10.1029/2008JD011023, 2009.

Ding, A. J., Fu, C. B., Yang, X. Q., Sun, J. N., Petäjä, T., Kerminen, V. M., Wang, T., Xie, Y., Herrmann, E., Zheng, L. F., Nie, W., Liu, Q., Wei, X. L. and Kulmala, M.: Intense atmospheric pollution modifies weather: A case of mixed biomass burning with fossil fuel combustion pollution in eastern China, Atmos. Chem. Phys., 13(20), 10545–10554, doi:10.5194/acp-13-10545-2013, 2013.

Dutot, A. L., Rynkiewicz, J., Steiner, F. E. and Rude, J.: A 24-h forecast of ozone peaks and exceedance levels using neural classifiers and weather predictions, Environ. Model. Softw., 22(9), 1261–1269, doi:10.1016/j.envsoft.2006.08.002, 2007.

Easter, R. C., Ghan, S. J., Zhang, Y., Saylor, R. D., Chapman, E. G., Laulainen, N. S., Abdul-Razzak, H., Leung, L. R., Bian, X. and Zaveri, R. A.: MIRAGE: Model description and evaluation of aerosols and trace gases, J. Geophys. Res. D Atmos., 109(20), doi:10.1029/2004JD004571, 2004.

Emmons, L. K., Walters, S., Hess, P. G., Lamarque, J.-F., Pfister, G. G., Fillmore, D., Granier, C., Guenther, A., Kinnison, D., Laepple, T., Orlando, J., Tie, X., Tyndall, G., Wiedinmyer, C., Baughcum, S. L. and Kloster, S.: Description and evaluation of the Model for Ozone and Related chemical Tracers, version 4 (MOZART-4), Geosci. Model Dev., 3(1), 43–67, doi:10.5194/gmd-3-43-2010, 2010.

Fan, J., Zhang, R., Li, G. and Tao, W. K.: Effects of aerosols and relative humidity on cumulus clouds, J. Geophys. Res. Atmos., 112(14), doi:10.1029/2006JD008136, 2007.

Fan, J., Zhang, R., Tao, W.-K. and Mohr, K. I.: Effects of aerosol optical properties on deep convective clouds and radiative forcing, J. Geophys. Res., 113(D8), D08209, doi:10.1029/2007JD009257, 2008.

Fan, J., Yuan, T., Comstock, J. M., Ghan, S., Khain, A., Leung, L. R., Li, Z., Martins, V. J. and Ovchinnikov, M.: Dominant role by vertical wind shear in regulating aerosol effects on deep convective clouds, J. Geophys. Res. Atmos., 114(22), doi:10.1029/2009JD012352, 2009.

Fan, J., Rosenfeld, D., Ding, Y., Leung, L. R. and Li, Z.: Potential aerosol indirect effects on atmospheric circulation and radiative forcing through deep convection, Geophys. Res. Lett., 39(9), doi:10.1029/2012GL051851, 2012.

Fan, J., Leung, L. R., Rosenfeld, D., Chen, Q., Li, Z., Zhang, J. and Yan, H.: Microphysical effects determine macrophysical response for aerosol impacts on deep convective clouds, Proc. Natl. Acad. Sci., 110(48), E4581–E4590, doi:10.1073/pnas.1316830110, 2013.

Fan, J., Rosenfeld, D., Yang, Y., Zhao, C., Leung, L. R. and Li, Z.: Substantial contribution of anthropogenic air pollution to catastrophic floods in Southwest China, Geophys. Res. Lett., n/a-n/a, doi:10.1002/2015GL064479, 2015.

Fast, J. D., Gustafson, W. I., Easter, R. C., Zaveri, R. A., Barnard, J. C., Chapman, E. G., Grell, G. A. and Peckham, S. E.: Evolution of ozone, particulates, and aerosol direct radiative forcing in the vicinity of Houston using a fully coupled meteorology-chemistry-aerosol model, J. Geophys. Res. Atmos., 111(21), 1–29, doi:10.1029/2005JD006721, 2006.

Fu, G., Yu, J., Yu, X., Ouyang, R., Zhang, Y., Wang, P., Liu, W. and Min, L.: Temporal variation of extreme rainfall events in China, 1961-2009, J. Hydrol., 487, 48–59, doi:10.1016/j.jhydrol.2013.02.021, 2013.

Graf, H. F.: The complex interaction of aerosols and clouds, Science, 303(5662), 1309–1311, doi:10.1126/science.1094411, 2004.

Grell, G., Freitas, S. R., Stuefer, M. and Fast, J.: Inclusion of biomass burning in WRF-Chem: Impact of wildfires on weather forecasts, Atmos. Chem. Phys., 11(11), 5289–5303, doi:10.5194/acp-11-5289-2011, 2011.

Grell, G. A., Peckham, S. E., Schmitz, R., McKeen, S. A., Frost, G., Skamarock, W. C. and Eder, B.: Fully coupled "online" chemistry within the WRF model, Atmos. Environ., 39(37), 6957–6975, doi:10.1016/j.atmosenv.2005.04.027, 2005.

Gu, Y. and Yim, S. H. L.: The air quality and health impacts of domestic trans-boundary pollution in various regions of China, Environ. Int., 97, 117–124, doi:10.1016/j.envint.2016.08.004, 2016.

Gunn, R. and Phillips, B. B.: An experimental investigation of the effect of air pollution on the Initiation of rain, J. Meteorol., 14, 272–279, 1957.

Guo, J., Deng, M., Lee, S. S., Wang, F., Li, Z., Zhai, P., Liu, H., Lv, W., Yao, W. and Li, X.: Delaying precipitation and lightning by air pollution over the pearl river delta. Part I: Observational analyses, J. Geophys. Res., 121(11), 6472–6488, doi:10.1002/2015JD023257, 2016a.

Guo, L., Turner, A. G. and Highwood, E. J.: Local and remote impacts of aerosol species on indian summer monsoon rainfall in a GCM, J. Clim., 29(19), 6937–6955, doi:10.1175/JCLI-D-15-0728.1, 2016b.

Guo J., Lou M., Miao Y., Wang Y., Zeng Z., Liu H., He J., Xu H., Wang F., Min M., and Zhai P.: Trans-Pacific transport of dust aerosol originated from East Asia: Insights gained from multiple observations and modeling, Environ. Poll., 230, 1030–1039, 10.1016/j.envpol.2017.07.062, 2017.

Gustafson, W. I., Chapman, E. G., Ghan, S. J., Easter, R. C. and Fast, J. D.: Impact on modeled cloud characteristics due to simplified treatment of uniform cloud condensation nuclei during NEAQS 2004, Geophys. Res. Lett., 34(19), L19809, doi:10.1029/2007GL030021, 2007.

Hansen, J., Sato, M. and Ruedy, R.: Radiative forcing and climate response, J. Geophys. Res., 102(D6), 6831–6864, doi:10.1029/96JD03436, 1997.

He, K., Huo, H. and Zhang, Q.: Urban air pollution in China: Current status, characteristics, and progress, Annu. Rev. Energy Environ., 27(1), 397–431, doi:10.1146/annurev.energy.27.122001.083421, 2002.

Hong, S.-Y., Noh, Y. and Dudhia, J.: A new vertical diffusion package with an explicit treatment of entrainment processes., Mon. Weather Rev., 134(9), 2318–2341, doi:10.1175/MWR3199.1, 2006.

Hu, Z., Zhao, C., Huang, J., Leung, L. R., Qian, Y., Yu, H., Huang, L. and Kalashnikova, O. V.: Trans-Pacific transport and evolution of aerosols: Evaluation of quasi-global WRF-Chem simulation with multiple observations, Geosci. Model Dev., 9(5), 1725–1746, doi:10.5194/gmd-9-1725-2016, 2016.

Iacono, M. J., Delamere, J. S., Mlawer, E. J., Shephard, M. W., Clough, S. A. and Collins, W. D.: Radiative forcing by long-lived greenhouse gases: Calculations with the AER radiative transfer models, , 113, 2–9, doi:10.1029/2008JD009944, 2008.

IPCC, 2013: Climate Change 2013: The physical science basis. Contribution of working Group I to the fifth assessment report of the Intergovernmental Panel on Climate Change [Stocker, T.F., D. Qin, G.-K. Plattner, M. Tignor, S.K. Allen, J. Boschung, A. Nauels, Y. Xia, V. Bex and P.M. Midgley (eds.)]. Cambridge University Press, Cambridge, United Kingdom and New York, NY, USA, 1535 pp, doi:10.1017/CBO9781107415324.

Janssens-Maenhout, G., Crippa, M., Guizzardi, D., Dentener, F., Muntean, M., Pouliot, G., Keating, T., Zhang, Q., Kurokawa, J., Wankmüller, R., Denier Van Der Gon, H., Kuenen, J. J. P., Klimont, Z., Frost, G., Darras, S., Koffi, B. and Li, M.: HTAP-v2.2: A mosaic of regional and global emission grid maps for 2008 and 2010 to study hemispheric transport of air pollution, Atmos. Chem. Phys., 15(19), 11411–11432, doi:10.5194/acp-15-11411-2015, 2015.

Jiang, Q., Li, W., Wen, J., Qiu, C., Sun, W., Fang, Q., Xu, M. and Tan, J.: Accuracy evaluation of two high-resolution satellite-based rainfall products: TRMM 3B42V7 and CMORPH in Shanghai, Water (Switzerland), 10(1), doi:10.3390/w10010040, 2018.

Jin, Q., Yang, Z. L. and Wei, J.: Seasonal responses of Indian summer monsoon to dust aerosols in the middle East, India, and China, J. Clim., 29(17), 6329–6349, doi:10.1175/JCLI-D-15-0622.1, 2016.

Joyce, R. J., Janowiak, J. E., Arkin, P. A. and Xie, P.: CMORPH: A method that produces global precipitation estimates from passive microwave and infrared data at high spatial and temporal resolution, J. Hydrometeorol., 5(3), 487–503, doi:10.1175/1525-7541(2004)005<0487:CAMTPG>2.0.CO;2, 2004.

Kain, J. S. and J. M. Fritsch: A one-dimensional entraining/detraining plume model and its application in convective parameterization, J. Atmos. Sci., 47, 2784–2802, doi.org/10.1175/1520-0469(1990)047<2784:AODEPM>2.0.CO;2, 1990.

Kaufman, Y. J. and Koren, I.: Smoke and pollution aerosol effect on cloud cover, Science, 313(5787), 655–658, doi:10.1126/science.1126232, 2006.

Khain, A., Rosenfeld, D. and Pokrovsky, A.: Aerosol impact on the dynamics and microphysics of deep convective clouds, Q. J. R. Meteorol. Soc., 131(611), 2639–2663, doi:10.1256/qj.04.62, 2005.

Khain, A. P.: Notes on state-of-the-art investigations of aerosol effects on precipitation: A critical review, Environ. Res. Lett., 4(1), doi:10.1088/1748-9326/4/1/015004, 2009.

Khain, A. P., BenMoshe, N. and Pokrovsky, A.: Factors determining the impact of aerosols on surface precipitation from clouds: An attempt at classification, J. Atmos. Sci., 65(6), 1721–1748, doi:10.1175/2007JAS2515.1, 2008.

Koren, I., Kaufman, Y. J., Remer, L. A. and Martins, J. V.: Measurement of the effect of amazon smoke on inhibition of cloud formation, Science, 303(5662), 1342–1345, doi:10.1126/science.1089424, 2004.

Koren, I., Vanderlei Martins, J., Remer, L. A. and Afargan, H.: Smoke invigoration versus inhibition of clouds over the amazon, Science, 321(5891), 946–949, doi:10.1126/science.1159185, 2008.

Koren, I., Feingold, G. and Remer, L. A.: The invigoration of deep convective clouds over the Atlantic: Aerosol effect, meteorology or retrieval artifact?, Atmos. Chem. Phys., 10(18), 8855–8872, doi:10.5194/acp-10-8855-2010, 2010.

Koren, I., Dagan, G. and Altaratz, O.: From aerosol-limited to invigoration of warm convective clouds, Science, 344(6188), 1143–1146, doi:10.1126/science.1252595, 2014.

Koren, I., Altaratz, O. and Dagan, G.: Aerosol effect on the mobility of cloud droplets, Environ. Res. Lett., 10(10), doi:10.1088/1748-9326/10/10/104011, 2015.

Lau, K. M. and Kim, K. M.: Observational relationships between aerosol and Asian monsoon rainfall, and circulation, Geophys. Res. Lett., 33(21), 1–5, doi:10.1029/2006GL027546, 2006.

Lee, S. S., Donner, L. J., Phillips, V. T. J. and Ming, Y.: The dependence of aerosol effect on clouds and precipitation on cloud-system organization, shear and stability, J. Geophys. Res. Atmos., 113(16), doi:10.1029/2007JD009224, 2008.

Li, G., Wang, Y. and Zhang, R.: Implementation of a two-moment bulk microphysics scheme to the WRF model to investigate

aerosol-cloud interaction, J. Geophys. Res. Atmos., 113(15), doi:10.1029/2007JD009361, 2008.

Li, Z., Niu, F., Fan, J., Liu, Y., Rosenfeld, D. and Ding, Y.: Long-term impacts of aerosols on the vertical development of clouds and precipitation, Nat. Geosci., 4(12), 888–894, doi:10.1038/ngeo1313, 2011.

Li Z., W.K.-M. Lau, V. Ramanathan, G. Wu, Y. Ding, M.G. Manoj, J. Liu, Y. Qian, J. Li, T. Zhou, J. Fan, D. Rosenfeld, Y. Ming, Y. Wang, J. Huang, B. Wang, X. Xu, S.-S., Lee, M. Cribb, F. Zhang, X. Yang, Takemura, K. Wang, X. Xia, Y. Yin, H. Zhang, J. Guo, P.M. Zhai, N. Sugimoto, S. S. Babu, G.P. Brasseur: Aerosol and monsoon climate interactions over Asia, Rev. Geophys., 54(4): 866–929, doi: 10.1002/2015RG000500, 2016.

Lin, J. C., Matsui, T., Pielke, S. A. and Kummerow, C.: Effects of biomass-burning-derived aerosols on precipitations and clouds in the Amazon Basin: A satellite-based empirical study, J. Geophys. Res. Atmos., 111(19), doi:10.1029/2005JD006884, 2006.

Liu, H., Jacob, D. J., Bey, I. and Yantosca, R. M.: Constraints from 210 Pb and 7 Be on wet deposition and transport in a global three-dimensional chemical tracer model driven by assimilated meteorological fields, J. Geophys. Res. Atmos., 106(D11), 12109–12128, doi:10.1029/2000JD900839, 2001.

Liu, Z., Yim, S. H. L., Wang, C. and Lau, N. C.: The impact of the aerosol direct radiative forcing on deep convection and air quality in the Pearl River Delta Region, Geophys. Res. Lett., doi:10.1029/2018GL077517, 2018.

Madronich, S.: Photodissociation in the atmosphere: 1. Actinic flux and the effects of ground reflections and clouds, J. Geophys. Res., 92(D8), 9740, doi:10.1029/JD092iD08p09740, 1987.

Morrison, H., Thompson, G. and Tatarskii, V.: Impact of cloud microphysics on the development of trailing stratiform precipitation in a simulated squall line: Comparison of one- and two-moment schemes, Mon. Weather Rev., 137(3), 991–1007, doi:10.1175/2008MWR2556.1, 2009.

Myhre, G., Myhre, C. E. L., Samset, B. H. and Storelvmo, T.: Aerosols and their relation to global climate and climate sensitivity, Nat. Educ. Knowl., 4(5):7, 1–15 [online] Available from: http://www.nature.com/scitable/knowledge/library/aerosols-and-their-relation-to-global-climate-102215345, 2013.

Otte, T. L., Pouliot, G., Pleim, J. E., Young, J. O., Schere, K. L., Wong, D. C., Lee, P. C. S., Tsidulko, M., McQueen, J. T., Davidson, P., Mathur, R., Chuang, H.-Y., DiMego, G. and Seaman, N. L.: Linking the eta model with the community multiscale air quality (CMAQ) modeling system to build a national air quality forecasting system, Weather Forecast., 20(3), 367–384, doi:10.1175/WAF855.1, 2005.

Qin, Y., Chen, Z., Shen, Y., Zhang, S. and Shi, R.: Evaluation of satellite rainfall estimates over the Chinese Mainland, Remote Sens., 6(11), 11649–11672, doi:10.3390/rs61111649, 2014.

Rosenfeld, D.: Suppression of rain and snow by urban and industrial air pollution, Science, 287(5459), 1793–1796, doi:10.1126/science.287.5459.1793, 2000.

Rosenfeld, D.: Aerosol-cloud interactions control of earth radiation and latent heat release budgets, Space Sci. Rev., 125(1–4), 149–157, doi:10.1007/s11214-006-9053-6, 2006.

Rosenfeld, D. and Woodley, W.: Deep convective clouds with sustained supercooled liquid water down to -37.5 degrees C,

Nature, 405(6785), 440–2, doi:10.1038/35013030, 2000.

Rosenfeld, D., Kaufman, Y. J. and Koren, I.: Switching cloud cover and dynamical regimes from open to closed Benard cells in response to the suppression of precipitation by aerosols, Atmos. Chem. Phys., 6(9), 2503–2511, doi:10.5194/acp-6-2503-2006, 2006.

Rosenfeld, D., Lohmann, U., Raga, G. B., O'Dowd, C. D., Kulmala, M., Fuzzi, S., Reissell, A. and Andreae, M. O.: Flood or drought: How do aerosols affect precipitation?, Science, 321(5894), 1309–1313, doi:10.1126/science.1160606, 2008.

Skamarock, W. C., Klemp, J. B., Dudhia, J., Gill, D. O., Barker, D. M., Duda, M. G., Huang, X.-Y., Wang, W. and Powers, J. G.: A description of the advanced research WRF version 3. [online] Available from: https://pdfs.semanticscholar.org/ace5/4d4d1d6c9914997ad8f4e410044fdeb95b9d.pdf (Accessed 15 May 2018), 2008.

Small, J. D., Chuang, P. Y., Feingold, G. and Jiang, H.: Can aerosol decrease cloud lifetime?, Geophys. Res. Lett., 36(16), doi:10.1029/2009GL038888, 2009.

Storer, R. L. and van den Heever, S. C.: Microphysical processes evident in aerosol forcing of tropical deep convective clouds, J. Atmos. Sci., 70(2), 430–446, doi:10.1175/JAS-D-12-076.1, 2013.

Tao, W. K., Li, X., Khain, A., Matsui, T., Lang, S. and Simpson, J.: Role of atmospheric aerosol concentration on deep convective precipitation: Cloud-resolving model simulations, J. Geophys. Res. Atmos., 112(24), doi:10.1029/2007JD008728, 2007.

Tao, W. K., Chen, J. P., Li, Z., Wang, C. and Zhang, C.: Impact of aerosols on convective clouds and precipitation, Rev. Geophys., 50(2), doi:10.1029/2011RG000369, 2012.

Twomey, S.: The Influence of pollution on the shortwave albedo of clouds, J. Atmos. Sci., 34(7), 1149–1152, doi:10.1175/1520-0469(1977)034<1149:TIOPOT>2.0.CO;2, 1977.

Wang, C.: A modeling study of the response of tropical deep convection to the increase of cloud condensation nuclei concentration: 1. Dynamics and microphysics, J. Geophys. Res. Atmos., 110(21), 1–16, doi:10.1029/2004JD005720, 2005.

Wang, Y., Wan, Q., Meng, W., Liao, F., Tan, H. and Zhang, R.: Long-term impacts of aerosols on precipitation and lightning over the Pearl River Delta megacity area in China, Atmos. Chem. Phys., 11(23), 12421–12436, doi:10.5194/acp-11-12421-2011, 2011.

Wiedinmyer, C., Akagi, S. K., Yokelson, R. J., Emmons, L. K., Al-Saadi, J. A., Orlando, J. J. and Soja, A. J.: The Fire INventory from NCAR (FINN) – a high resolution global model to estimate the emissions from open burning, Geosci. Model Dev. Discuss., 3(4), 2439–2476, doi:10.5194/gmdd-3-2439-2010, 2010.

Wu, D., Tie, X., Li, C., Ying, Z., Lau, A. K. H., Huang, J., Deng, X. and Bi, X.: An extremely low visibility event over the Guangzhou region: A case study, Atmos. Environ., 39(35), 6568–6577, doi:10.1016/j.atmosenv.2005.07.061, 2005.

Xie, P., Joyce, R., Wu, S., Yoo, S.-H., Yarosh, Y., Sun, F. and Lin, R.: Reprocessed, bias-corrected CMORPH global high-resolution precipitation estimates from 1998, J. Hydrometeorol., 18(6), 1617–1641, doi:10.1175/JHM-D-16-0168.1, 2017.

Yang, Q., Gustafson, W. I., Fast, J. D., Wang, H., Easter, R. C., Morrison, H., Lee, Y. N., Chapman, E. G., Spak, S. N. and Mena-Carrasco, M. A.: Assessing regional scale predictions of aerosols, marine stratocumulus, and their interactions during

VOCALS-REx using WRF-Chem, Atmos. Chem. Phys., 11(23), 11951–11975, doi:10.5194/acp-11-11951-2011, 2011.

Zaveri, R. A. and Peters, L. K.: A new lumped structure photochemical mechanism for large-scale applications, J. Geophys. Res. Atmos., 104(D23), 30387–30415, doi:10.1029/1999JD900876, 1999.

Zaveri, R. A., Easter, R. C., Fast, J. D. and Peters, L. K.: Model for simulating aerosol interactions and chemistry (MOSAIC), J. Geophys. Res. Atmos., 113(13), doi:10.1029/2007JD008782, 2008.

Zhang, Y. L., and F. Cao: Fine particulate matter ($PM_{2.5}$) in China at a city level. Sci. Rep., 5, 14884, https://doi.org/10.1038/srep14884, 2015.

Zhao, C., Wang, Y., Choi, Y. and Zeng, T.: Summertime impact of convective transport and lightning NOx production over North America: Modeling dependence on meteorological simulations, Atmos. Chem. Phys., 9(13), 4315–4327, doi:10.5194/acp-9-4315-2009, 2009.

Zhao, C., Liu, X., Leung, L. R., Johnson, B., Mcfarlane, S. A., Jr, W. I. G., Fast, J. D. and Easter, R.: The spatial distribution of mineral dust and its shortwave radiative forcing over North Africa: modeling sensitivities to dust emissions and aerosol size treatments, Atmos. Chem. Phys., 10, 8821–8838, doi:10.5194/acp-10-8821-2010, 2010.

Zhao, C., Liu, X., Leung, L. R. and Hagos, S.: and Physics Radiative impact of mineral dust on monsoon precipitation variability over West Africa, (2007), 1879–1893, doi:10.5194/acp-11-1879-2011, 2011.

Zhao, C., Leung, L. R., Easter, R., Hand, J. and Avise, J.: Characterization of speciated aerosol direct radiative forcing over California, J. Geophys. Res. Atmos., 118(3), 2372–2388, doi:10.1029/2012JD018364, 2013a.

Zhao, C., Chen, S., Leung, L. R., Qian, Y., Kok, J. F., Zaveri, R. A. and Huang, J.: Uncertainty in modeling dust mass balance and radiative forcing from size parameterization, Atmos. Chem. Phys., 13(21), 10733–10753, doi:10.5194/acp-13-10733-2013, 2013b.

Zhao, C., Hu, Z., Qian, Y., Ruby Leung, L., Huang, J., Huang, M., Jin, J., Flanner, M. G., Zhang, R., Wang, H., Yan, H., Lu, Z. and Streets, D. G.: Simulating black carbon and dust and their radiative forcing in seasonal snow: A case study over North China with field campaign measurements, Atmos. Chem. Phys., 14(20), 11475–11491, doi:10.5194/acp-14-11475-2014, 2014.

Zhao, C., Huang, M., Fast, J. D., Berg, L. K., Qian, Y., Guenther, A., Gu, D., Shrivastava, M., Liu, Y., Walters, S., Pfister, G., Jin, J., Shilling, J. E. and Warneke, C.: Sensitivity of biogenic volatile organic compounds to land surface parameterizations and vegetation distributions in California, Geosci. Model Dev., 9(5), 1959–1976, doi:10.5194/gmd-9-1959-2016, 2016.

Zhong, S., Qian, Y., Zhao, C., Leung, R. and Yang, X. Q.: A case study of urbanization impact on summer precipitation in the greater Beijing metropolitan area: Urban heat island versus aerosol effects, J. Geophys. Res., 120(20), 10,903-10,914, doi:10.1002/2015JD023753, 2015.

Zhong, S., Qian, Y., Zhao, C., Leung, R., Wang, H., Yang, B., Fan, J., Yan, H., Yang, X. Q. and Liu, D.: Urbanization-induced urban heat island and aerosol effects on climate extremes in the Yangtze River Delta region of China, Atmos. Chem. Phys., 17(8), 5439–5457, doi:10.5194/acp-17-5439-2017, 2017.

Atmos. Chem. Phys. Discuss., https://doi.org/10.5194/acp-2018-977
Manuscript under review for journal Atmos. Chem. Phys.
Discussion started: 4 October 2018

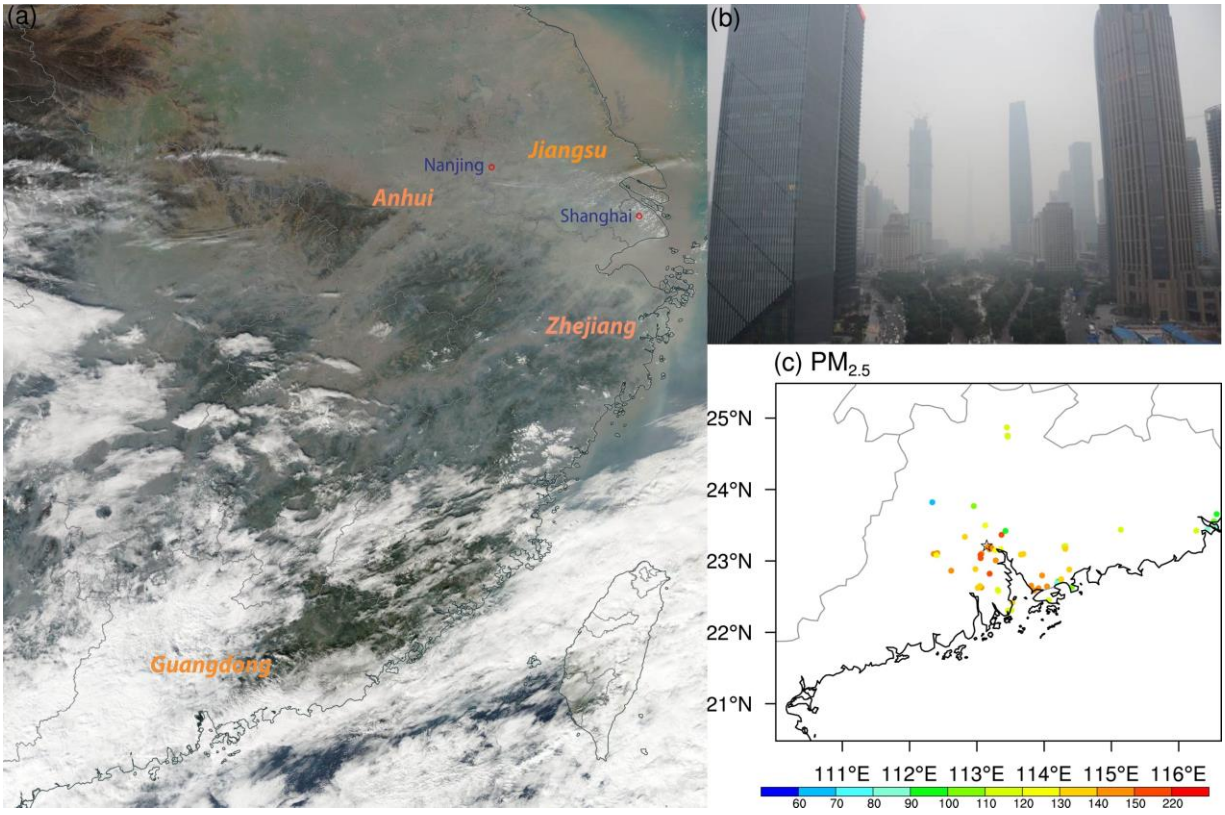

Figure 1. (a) Terra satellite true-color image of east China on December 13, 2013 (UTC), provided by NASA's Worldview (source: https://worldview.earthdata.nasa.gov/). Red circles denote city locations, blue fonts denote cities, and orange fonts in bold italic denote provinces. (b) Photo of Canton Tower taken by Lin Longyong in the afternoon of December 13, 2013 (source: https://3g.163.com/fashion/article/9HJVQL9C00264MP0.html). (c) Hourly-averaged $PM_{2.5}$ (unit: μg m^{-3}) concentration on December 13, 2013, observed in Guangdong province. Colored circles denote in situ station locations, and black star denotes Guangzhou.

Atmos. Chem. Phys. Discuss., https://doi.org/10.5194/acp-2018-977
Manuscript under review for journal Atmos. Chem. Phys.
Discussion started: 4 October 2018

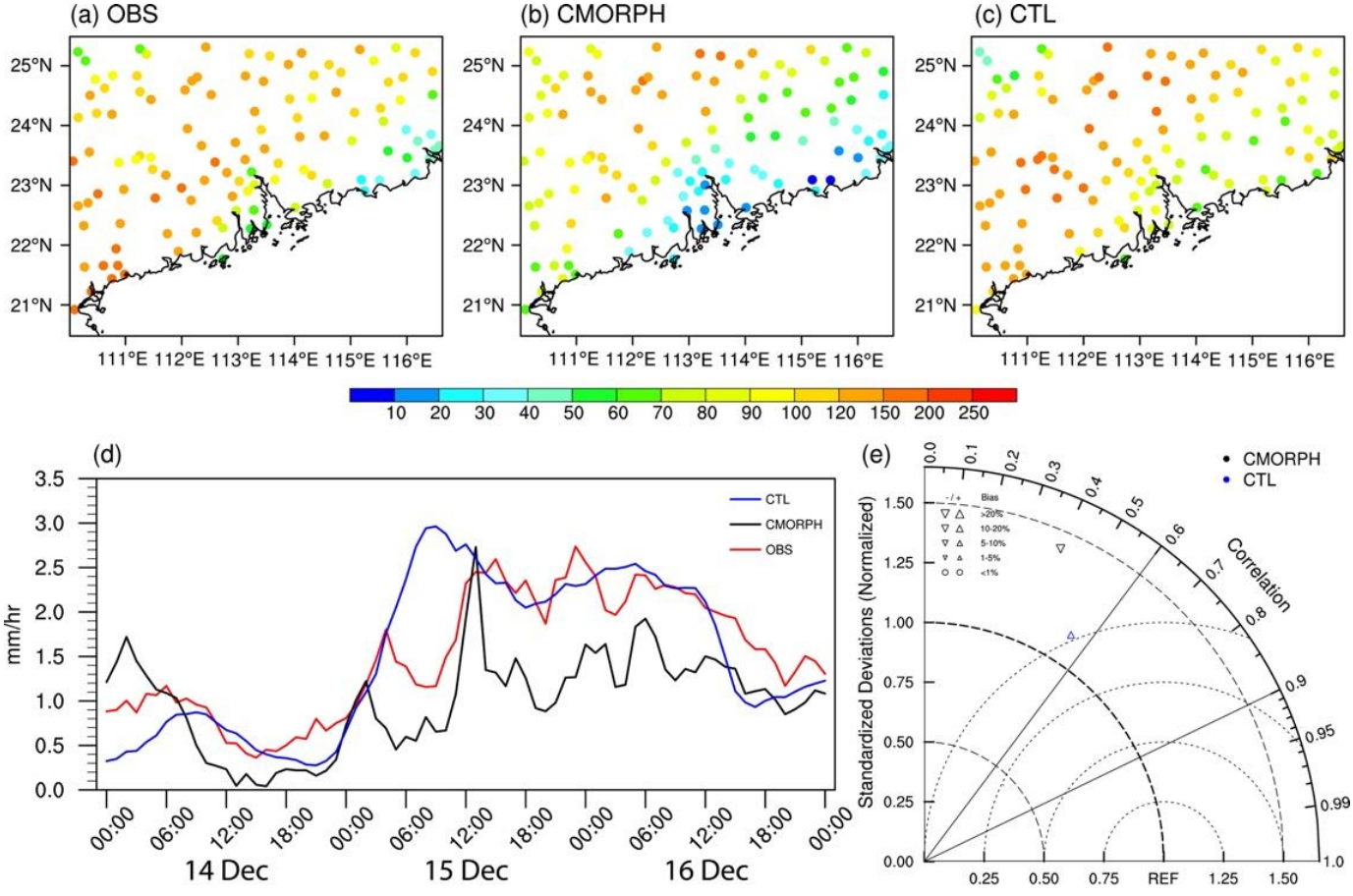

Figure 2. Spatial distribution of accumulated precipitation (unit: mm) from 00Z on December 14, 2013, to 00Z on December 17, 2013 (local standard time [LST]) from (a) station observations (OBS), (b) CMORPH satellite, (c) control simulation (CTL). Circles denote locations of in situ observations. (d) Time series of station average of rain rate (unit: mm h^{-1}) over the entire domain 2 for OBS (red), CMORPH (black), and CTL (blue). (e) Taylor diagrams for 3-day accumulated precipitation in CTL (blue) and CMORPH (black) compared with OBS. Triangles and circles at top-left corner in (e) denote bias. Sizes of triangles indicate magnitude of bias. Inverted (upright) triangles represent a negative (positive) bias.

Atmos. Chem. Phys. Discuss., https://doi.org/10.5194/acp-2018-977
Manuscript under review for journal Atmos. Chem. Phys.
Discussion started: 4 October 2018

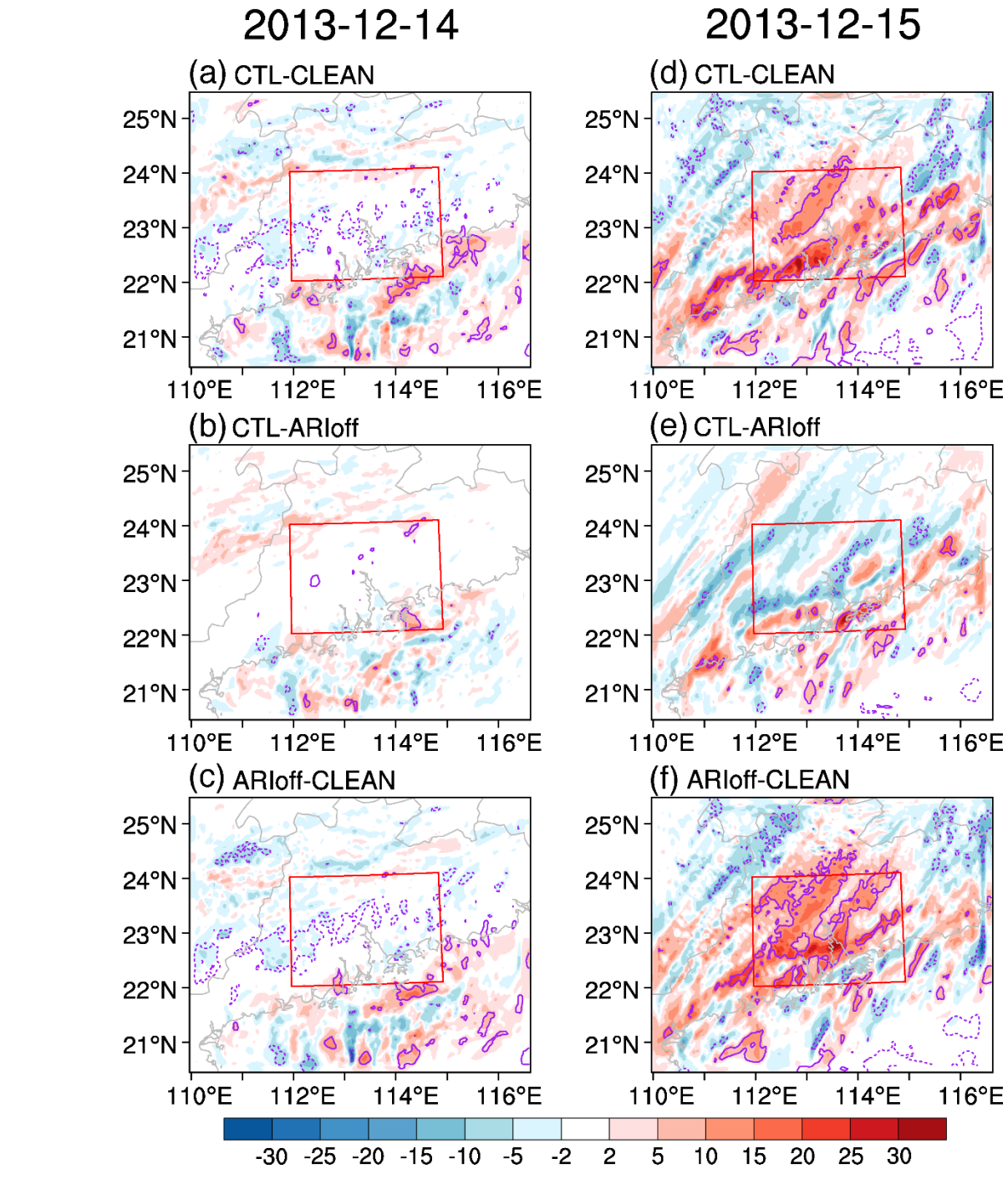

Figure 3. Differences in precipitation (unit: mm) between CTL and CLEAN (i.e., CTL minus CLEAN; first row), CTL and ARIoff (i.e., CTL minus ARIoff; second row), and ARIoff and CLEAN (i.e., ARIoff minus CLEAN; third row) on December 14 (left column) and December 15 (right column). Solid (dashed) purple contour lines indicate positive (negative) differences at the 90% significance level according to two-tailed Student's *t* test. Red boxes (22°–24° N, 112°–115° E) denote the analysis region. ARIoff run refers to simulation with aerosol-radiation interactions off.

Atmos. Chem. Phys. Discuss., https://doi.org/10.5194/acp-2018-977
Manuscript under review for journal Atmos. Chem. Phys.
Discussion started: 4 October 2018

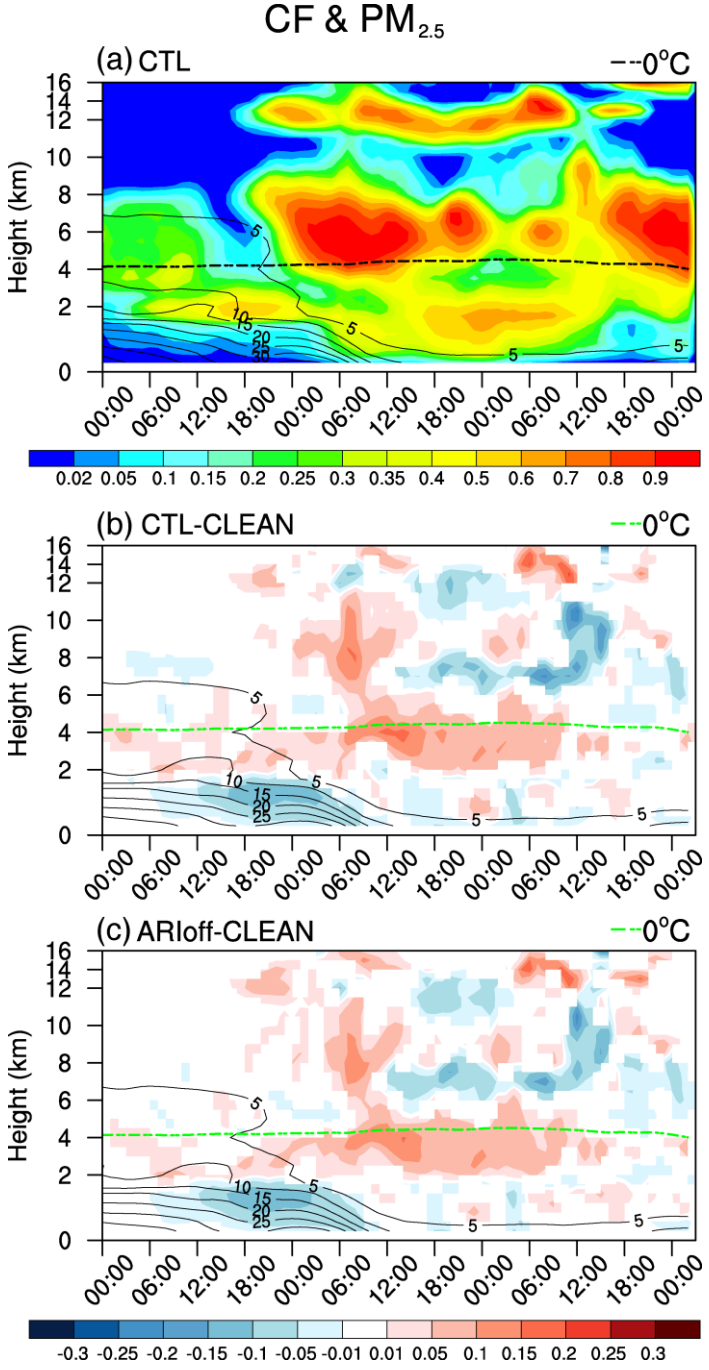

Figure 4. (a) Time–height cross section of cloud fraction (CF; shading; unit: unitless) and $PM_{2.5}$ concentrations (contour; contour interval [CI]: 5 μg m^{-3}) averaged over the red box shown in Figure 3 in CTL run. Differences in the time–height cross section of CF (shading; unit: unitless) and $PM_{2.5}$ concentration (contour; CI: 5 μg m^{-3}) averaged over the red box shown in Figure 3 between (b) CTL and CLEAN (i.e., CTL minus CLEAN) and (c) ARIoff and CLEAN (i.e., ARIoff minus CLEAN). In (b) and (c), only CF and $PM_{2.5}$ concentrations anomalies that exceed the 90% significance level are depicted with shading and contour, respectively. Dashed lines denote 0°C isotherm calculated as the averaged zero-layer height over the red box in Figure 3.

Atmos. Chem. Phys. Discuss., https://doi.org/10.5194/acp-2018-977
Manuscript under review for journal Atmos. Chem. Phys.
Discussion started: 4 October 2018

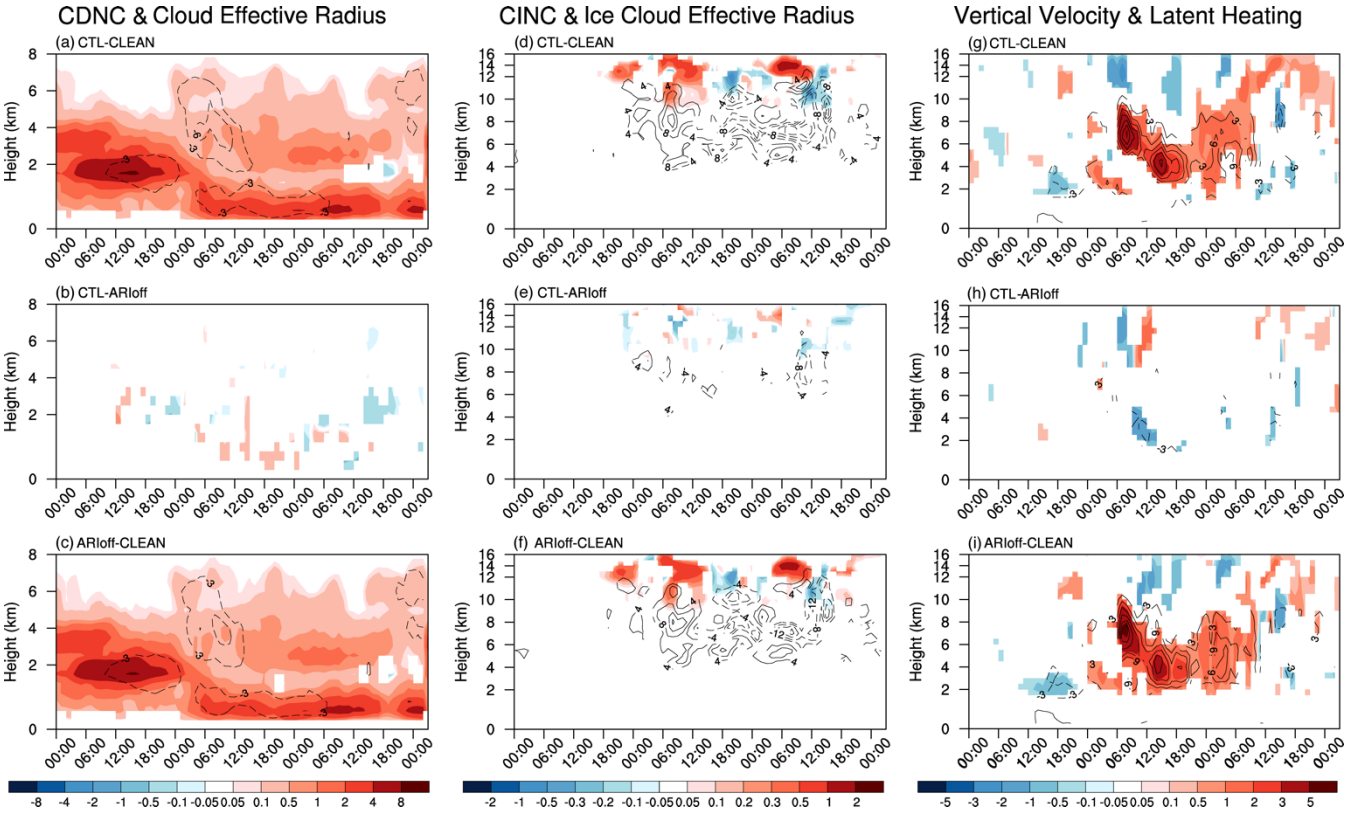

Figure 5. Differences with time (abscissa; from 00Z on December 14 to 02Z on December 17) and height (ordinate) in (left column) cloud droplet number concentration (CDNC, shading; unit: 10^7 kg^{-1}) and cloud effective radius (contour; CI: 3 μm), (middle column) cloud ice number concentration (CINC, shading; unit: 10^5 kg^{-1}) and ice cloud effective radius (contour; CI: 4 μm), and (right column) vertical velocity (shading; unit: cm s^{-1}) and latent heating (contour; CI: 3 K d^{-1}) averaged over the red box shown in Figure 3 between CTL and CLEAN (i.e., CTL minus CLEAN; first row), CTL and ARIoff (i.e., CTL minus ARIoff; second row), and ARIoff and CLEAN (i.e., ARIoff minus CLEAN; third row). Only anomalies that exceed the 90% significance level are depicted with shading or contour. Zero-value contour lines are omitted, and negative values are dashed.

Atmos. Chem. Phys. Discuss., https://doi.org/10.5194/acp-2018-977
Manuscript under review for journal Atmos. Chem. Phys.
Discussion started: 4 October 2018

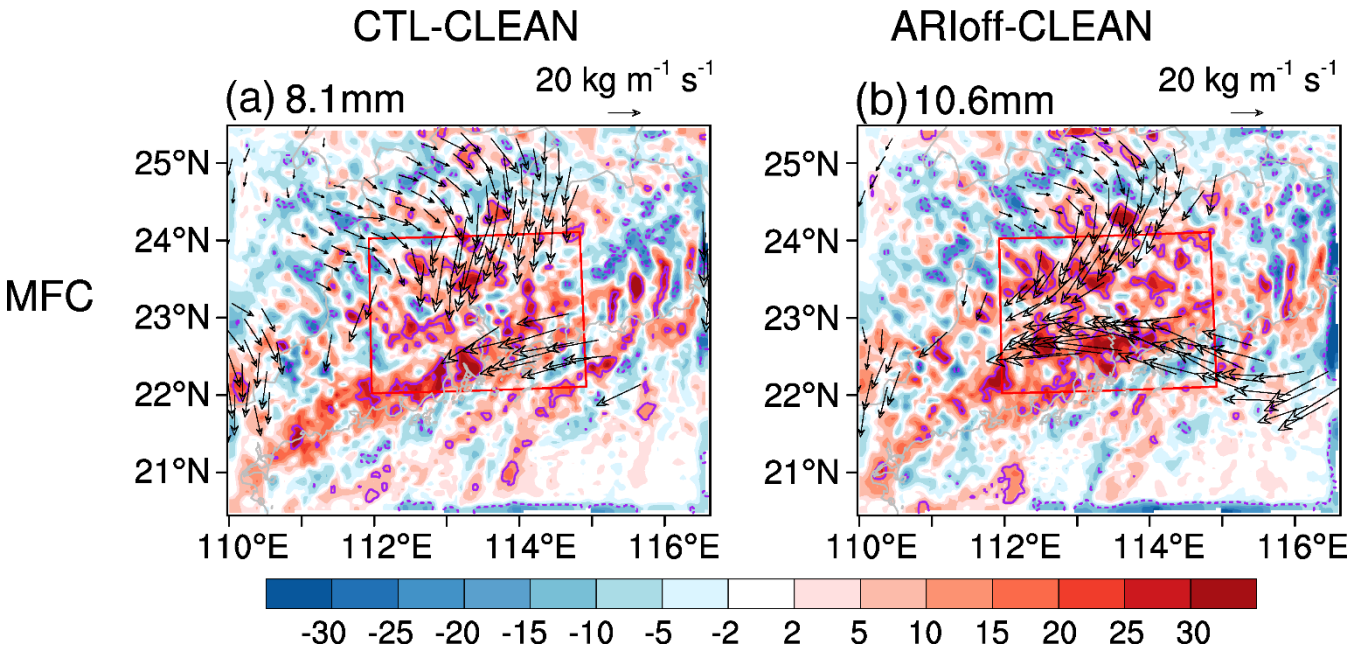

Figure 6. Differences in column-integrated flux convergence (MFC; shading; unit: mm) and moisture flux (vector; unit: kg m^{-1} s^{-1}) between CTL and CLEAN (i.e., CTL minus CLEAN; left column) and ARIoff and CLEAN (i.e., ARIoff minus CLEAN; right column) on December 15. Solid (dashed) purple contour lines indicate positive (negative) differences (shading) at the 90% significance level according to two-tailed Student's *t* test. Only moisture flux anomalies that exceed the 90% significance level are depicted with black vectors. Numbers at top-left corner of each panel represent values averaged over red boxes. Red boxes (22°–24° N, 112°–115° E) denote the analysis region.

Atmos. Chem. Phys. Discuss., https://doi.org/10.5194/acp-2018-977
Manuscript under review for journal Atmos. Chem. Phys.
Discussion started: 4 October 2018

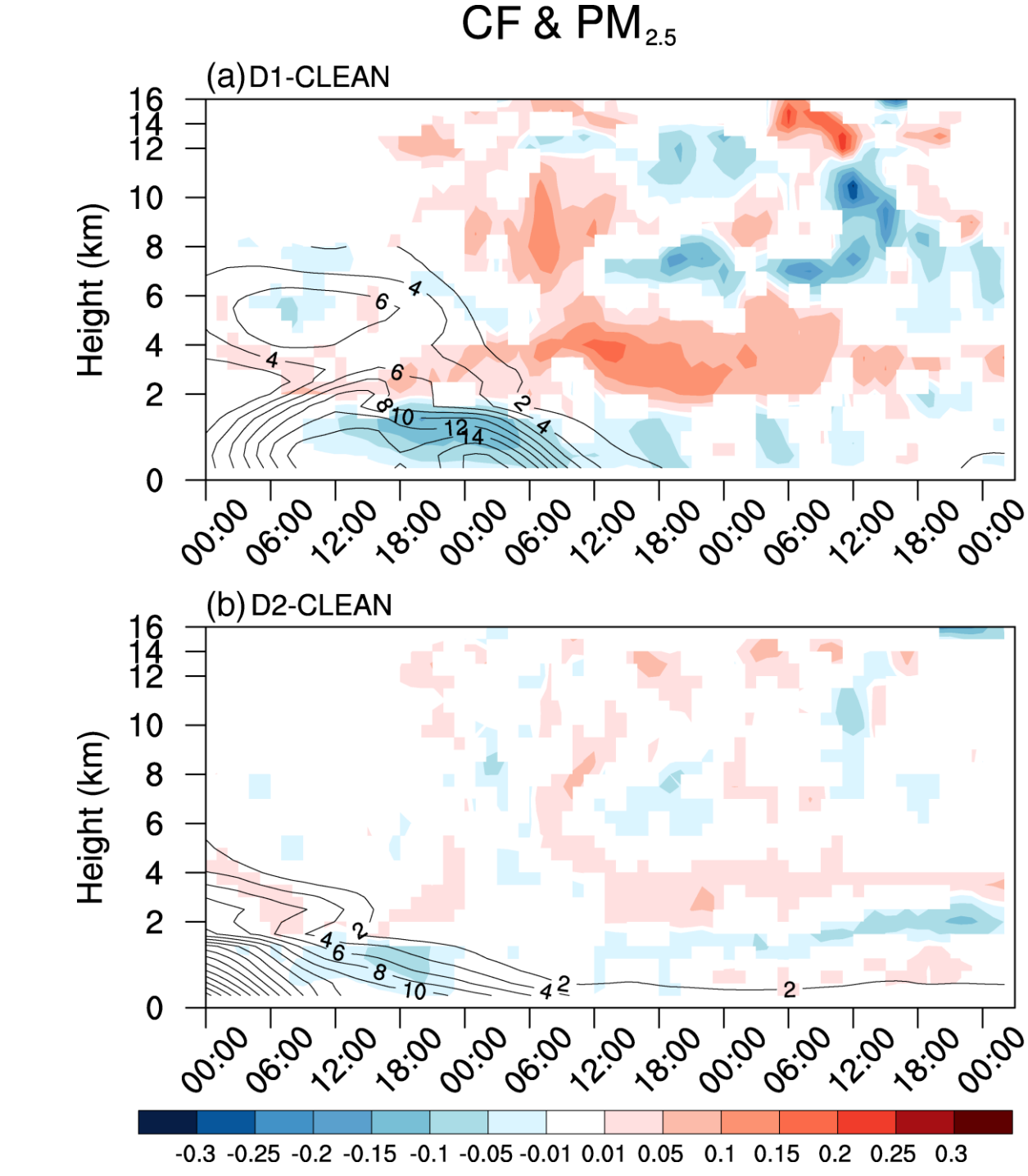

Figure 7. Differences in time–height cross section of CF (shading; unit: unitless) and $PM_{2.5}$ concentration (contour; CI: 2 μg m^{-3}) averaged over the red box shown in Figure 3 between (a) D1 and CLEAN (i.e., D1 minus CLEAN) and (b) D2 and CLEAN (i.e., D2 minus CLEAN). Only CF and $PM_{2.5}$ concentrations anomalies that exceed the 90% significance level are depicted with shading and contour, respectively.

Atmos. Chem. Phys. Discuss., https://doi.org/10.5194/acp-2018-977
Manuscript under review for journal Atmos. Chem. Phys.
Discussion started: 4 October 2018

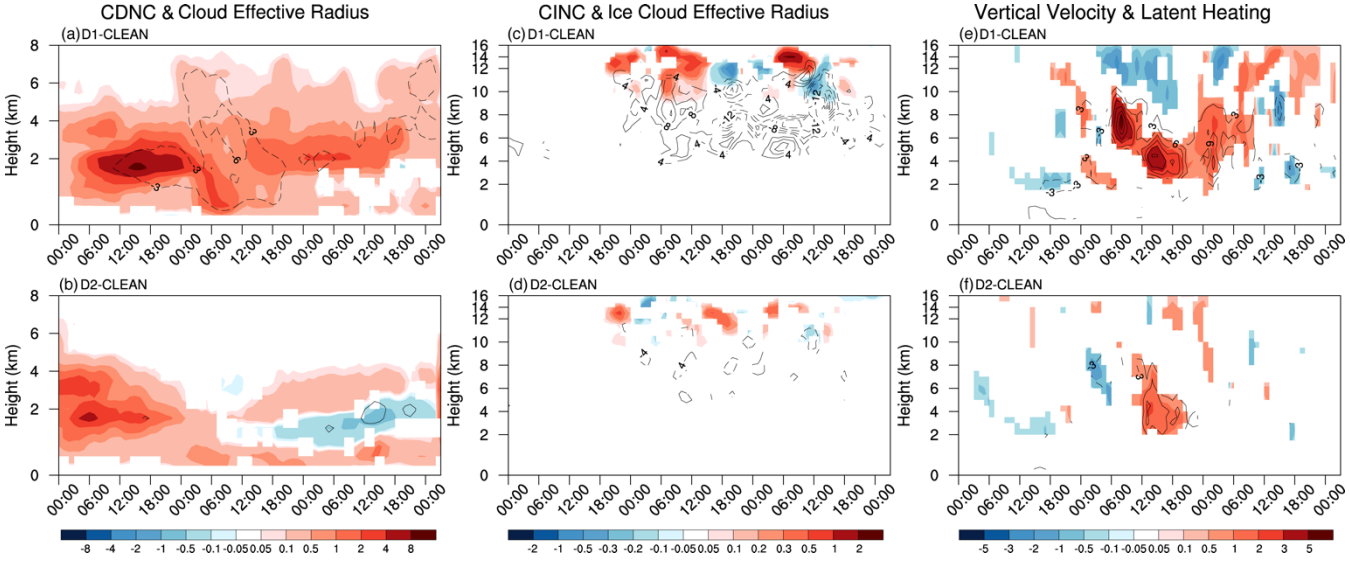

Figure 8. Differences with time (abscissa; from 00Z on December 14 to 02Z on December 17) and height (ordinate) in (left column) CDNC (shading; unit: 10^7 kg^{-1}) and cloud effective radius (contour; CI: 3 μm), (middle column) CINC (shading; unit: 10^5 kg^{-1}) and ice cloud effective radius (contour; CI: 4 μm), and (right column) vertical velocity (shading; unit: cm s^{-1}) and latent heating (contour; CI: 3 K d^{-1}) averaged over the red box shown in Figure 3 between D1 and CLEAN (i.e., D1 minus CLEAN; first row) and D2 and CLEAN (i.e., D2 minus CLEAN; second row). Only anomalies that exceed the 90% significance level are depicted with shading or contour. Zero-value contour lines are omitted, and negative values are dashed.

Atmos. Chem. Phys. Discuss., https://doi.org/10.5194/acp-2018-977
Manuscript under review for journal Atmos. Chem. Phys.
Discussion started: 4 October 2018

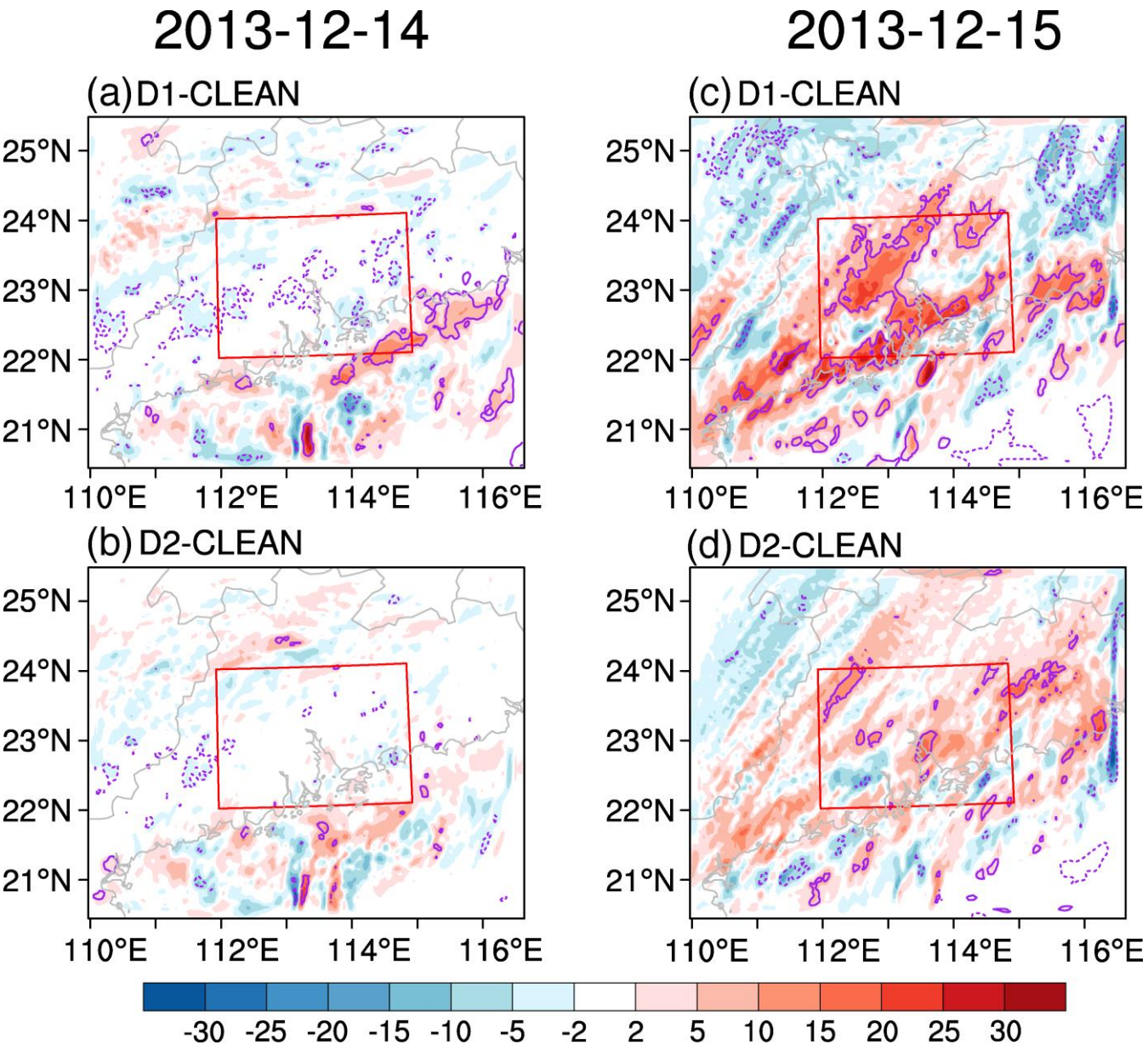

Figure 9. Differences in precipitation (unit: mm) between D1 and CLEAN (i.e., D1 minus CLEAN; first row) and D2 and CLEAN (i.e., D2 minus CLEAN; second row) on December 14 (left column) and December 15 (right column). Solid (dashed) purple contour lines indicate positive (negative) differences at the 90% significance according to two-tailed Student's *t* test. Red boxes (22°–24° N, 112°–115° E) denote the analysis region.

Atmos. Chem. Phys. Discuss., https://doi.org/10.5194/acp-2018-977
Manuscript under review for journal Atmos. Chem. Phys.
Discussion started: 4 October 2018

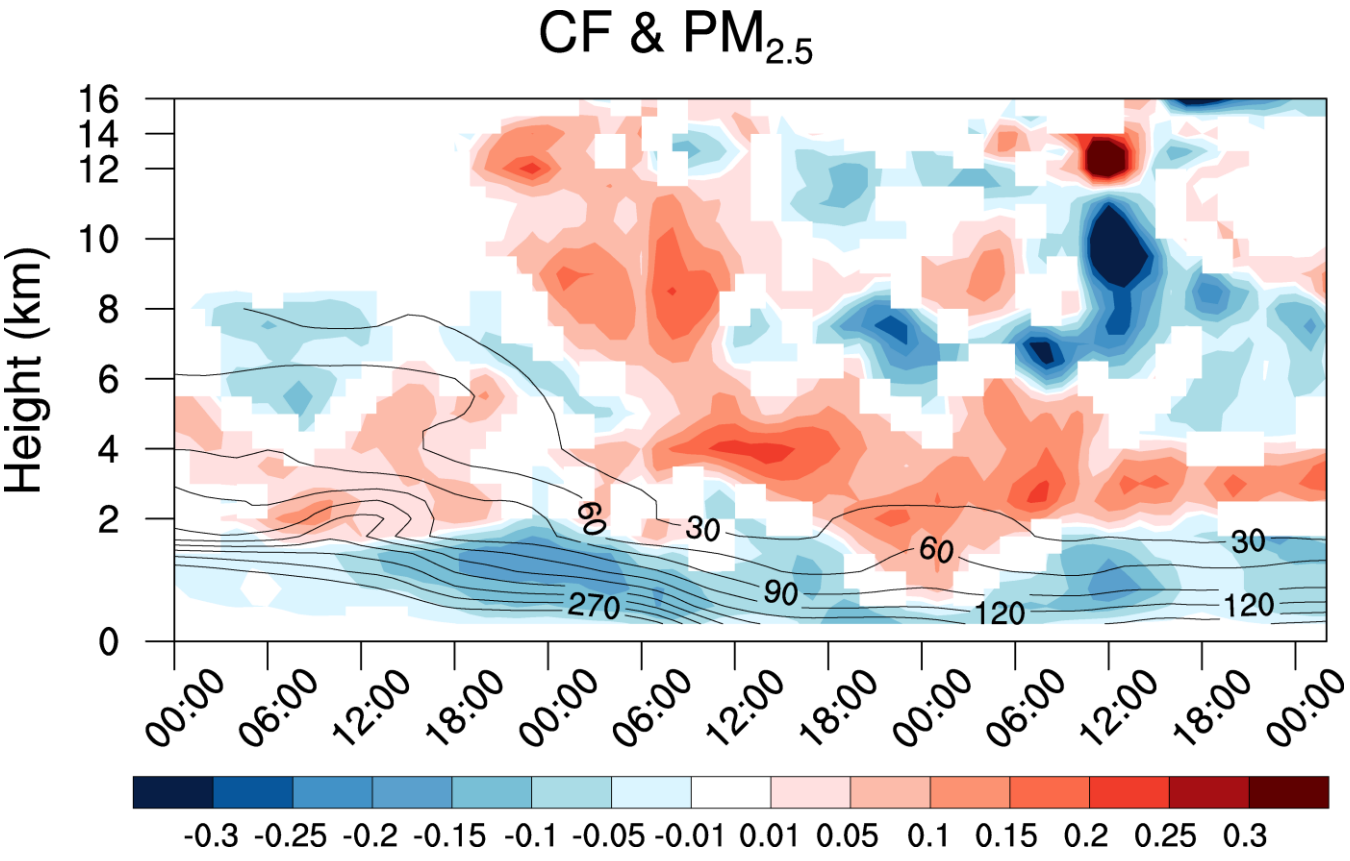

Figure 10. Differences in the time–height cross section of cloud factor CF (shading; unit: unitless) and $PM_{2.5}$ concentrations (contour; CI: 30 μg m^{-3}) averaged over the red box shown in Figure 3 between 10× and CLEAN (i.e., 10× minus CLEAN). Only CF and $PM_{2.5}$ concentrations anomalies that exceed the 90% significance level are depicted with shading and contour, respectively.

Atmos. Chem. Phys. Discuss., https://doi.org/10.5194/acp-2018-977
Manuscript under review for journal Atmos. Chem. Phys.
Discussion started: 4 October 2018

Atmospheric Chemistry and Physics Discussions

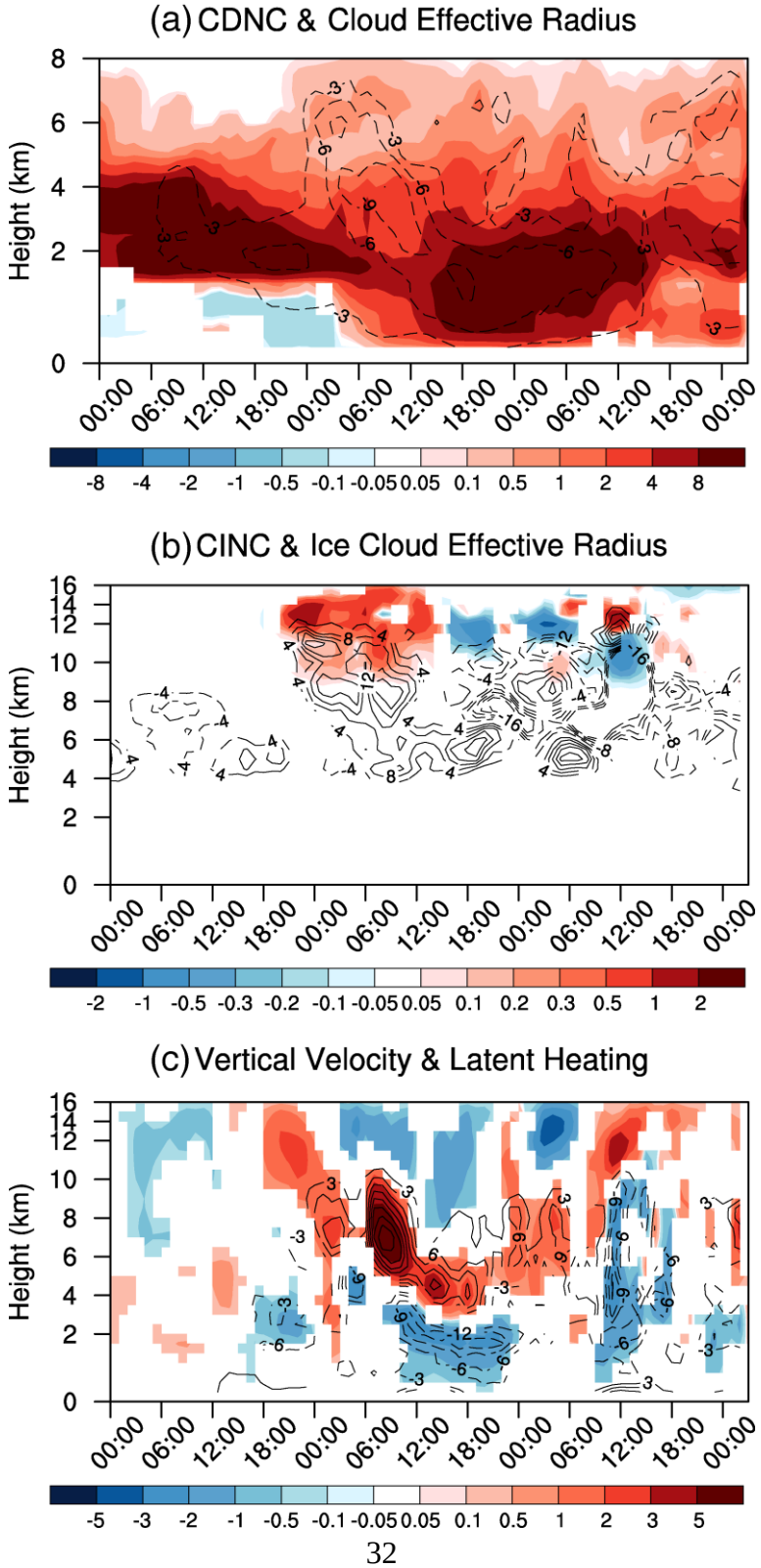

Atmos. Chem. Phys. Discuss., https://doi.org/10.5194/acp-2018-977
Manuscript under review for journal Atmos. Chem. Phys.
Discussion started: 4 October 2018

Atmospheric Chemistry and Physics Discussions

Figure 11. Differences with time (abscissa; from 00Z on December 14 to 02Z on December 17) and height (ordinate) in (a) CDNC (shading; unit: 10^7 kg^{-1}) and cloud effective radius (CI: 3 μm), (b) CINC (shading; unit: 10^5 kg^{-1}) and ice cloud effective radius (contour; CI: 4 μm), and (c) vertical velocity (shading; unit: cm s^{-1}) and latent heating (contour; CI: 3 K d^{-1}) averaged over the red box shown in Figure 3 between 10× and CLEAN (i.e., 10× minus CLEAN). Only anomalies that exceed the 90% significance level are depicted with shading or contour. Zero-value contour lines are omitted, and negative values are dashed.

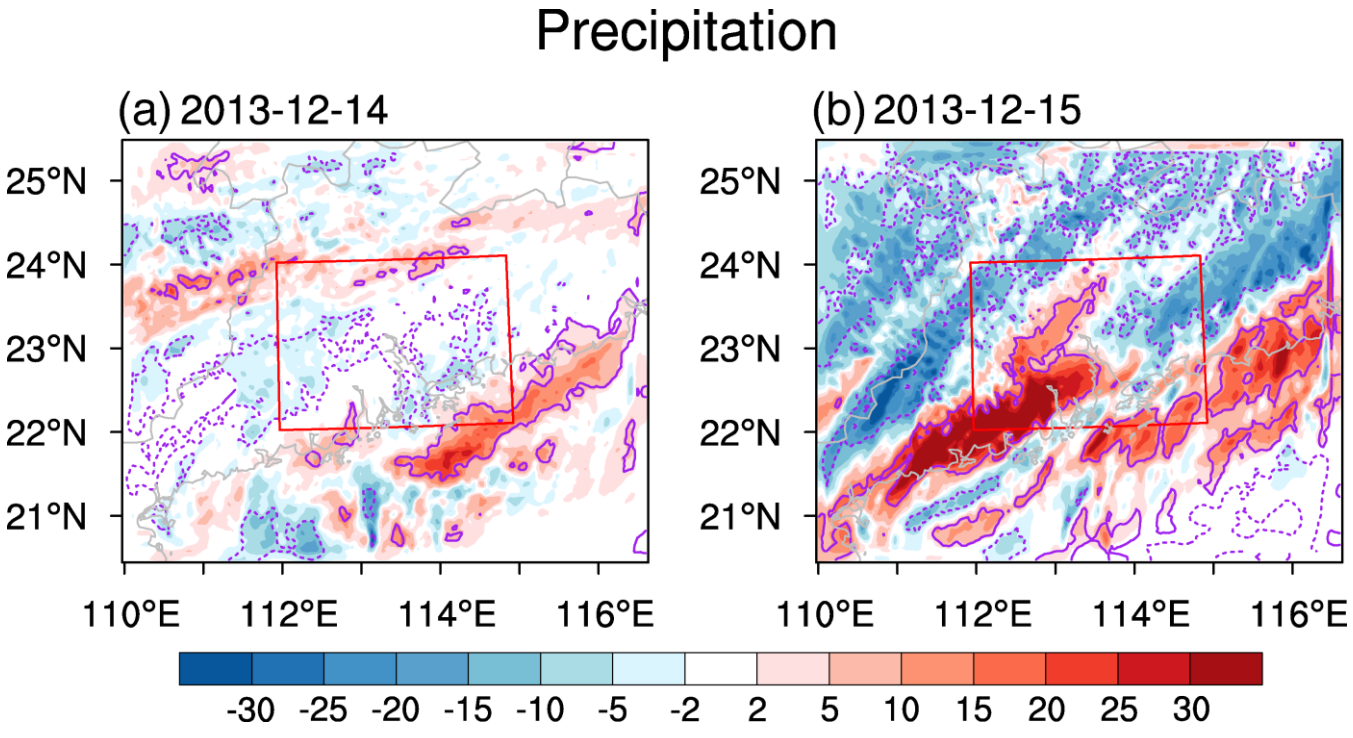

Figure 12. Differences in precipitation (unit: mm) between 10× and CLEAN (i.e., 10× minus CLEAN) on December 14 (left) and December 15 (right). Solid (dashed) purple contour lines indicate positive (negative) differences at the 90% significance according to two-tailed Student's *t* test. Red boxes (22°–24° N, 112°–115° E) denote the analysis region.

Atmos. Chem. Phys. Discuss., https://doi.org/10.5194/acp-2018-977
Manuscript under review for journal Atmos. Chem. Phys.
Discussion started: 4 October 2018

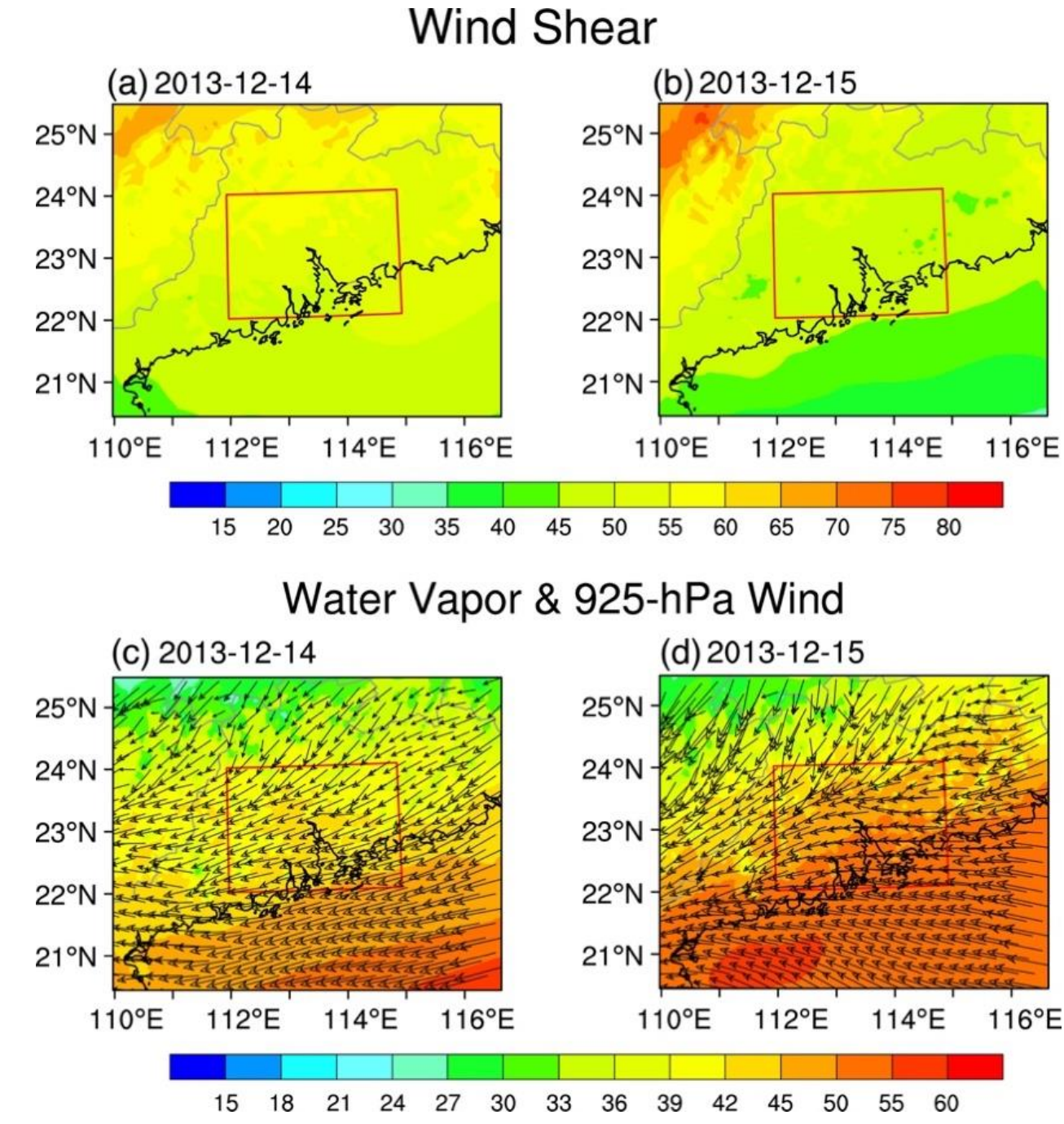

Figure 13. Spatial distribution of wind shear (unit: m s^{-1}) on (a) December 14 and (b) December 15 in 2013 in the CTL run (first row). Wind shear is calculated as differences between maximum wind speed and minimum wind speed at 0–10 km. Spatial distribution of column-integrated water vapor (shading; unit: mm day^{-1}) and 925-hPa wind (vector; unit: m s^{-1}) on (c) December 14 and (d) December 15 in 2013 in CTL (second row). Red boxes (22°–24° N, 112°–115° E) denote the analysis region.

Atmos. Chem. Phys. Discuss., https://doi.org/10.5194/acp-2018-977
Manuscript under review for journal Atmos. Chem. Phys.
Discussion started: 4 October 2018

Atmospheric Chemistry and Physics Discussions

Table 1. Model simulations. Abbreviations: CTL, control run; ARIoff, turn off aerosol-radiation interactions; D1, keep emissions in domain 1 as control run while make those except for chemical boundary conditions in domain 2 as CLEAN run; D2, keep emissions and chemical initial conditions in domain 2 as control run, make those and chemical boundary conditions in domain 1 as CLEAN run; 10×, tenfold of anthropogenic emissions and chemical initial and boundary conditions. * indicates that emissions, initial conditions (ICs), or boundary conditions (BCs), are scaled from the control run. Note the offline chemical BCs here were extracted from global chemical transport models and only used for domain 1.

Simulation	Anthropogenic and fire emissions, chemical ICs and BCs*		Aerosol-radiation interactions	Aerosol-cloud interactions
	Domain 1	Domain 2		
CTL	1	1	Yes	Yes
ARIoff	1	1	No	Yes
CLEAN	0.1	0.1	Yes	Yes
D1	1	0.1	Yes	Yes
D2	0.1	1	Yes	Yes
10×	10	10	Yes	Yes